

NUMERICAL INVESTIGATION OF RADIATIVE OPTICALLY-DENSE TRANSIENT MAGNETIZED REACTIVE TRANSPORT PHENOMENA WITH CROSS DIFFUSION, DISSIPATION AND WALL MASS FLUX EFFECTS

O. Anwar Bég¹, M. Ferdows², Eeman T. A. Bég³, T. Ahmed⁴, M. Wahiduzzaman⁴ and Md. M. Alam²

¹Spray Research Group, School of Computing, Science and Engineering, Newton Bldg, The Crescent, University of Salford, Manchester, M54WT, England, UK.

²Department of Applied Mathematics, University of Dhaka, Dhaka-1000, Bangladesh.

³Renewable Energy Research, Israfil House, Dickenson Rd., Manchester, M13, UK.

⁴Mathematics Discipline, Khulna University, Khulna-9208, Bangladesh

Abstract

High temperature electromagnetic materials fabrication systems in chemical engineering require ever more sophisticated theoretical and computational models for describing multiple, simultaneous thermophysical effects. Motivated by this application, the present article addresses transient magnetohydrodynamic heat and mass transfer in chemically-reacting fluid flow from an impulsively-started vertical perforated sheet. Thermal radiation flux, internal heat generation (heat source), Joule magnetic heating (Ohmic dissipation), thermo-diffusive and diffusio-thermal (i.e. cross-diffusion) effects and also viscous dissipation are incorporated in the mathematical model. To facilitate numerical solutions of the coupled, nonlinear boundary value problem, non-similar transformations are employed and the partial differential conservation equations are normalized into a dimensionless system of momentum, energy and concentration equations with associated boundary thermal conditions. An implicit finite difference method (FDM) is utilized to solve the unsteady equations. Verification of the FDM solutions for dimensionless velocity, temperature and concentration functions is achieved with a variational finite element method code (MAGNETO-FEM) and also a network simulation method code (MAG-PSPICE). The influence of the emerging thermo-physical parameters on transient velocity, temperature, concentration, wall shear stress, Nusselt number and Sherwood number is elaborated. The flow is accelerated with increasing thermal radiative flux, Eckert number, heat generation and Soret number whereas the flow is decelerated with greater wall suction, heat absorption, magnetic field and Prandtl number. Temperatures are also observed to be elevated with magnetic parameter, radiation heat transfer, Dufour number, heat generation (source) and Eckert number with the contrary effects computed for increasing suction parameter or Prandtl number. The species concentration is enhanced with Soret number and generative chemical reaction whereas it is depressed with greater wall suction, Schmidt number and destructive chemical reaction parameter

Keywords: Unsteady radiation magnetohydrodynamics; Soret and Dufour effects; Chemical reaction; magnetic materials processing; Numerical solutions; Ohmic dissipation.

[^]Corresponding author- email: gortoab@gmail.com; O.A.Beg@salford.ac.uk

1. INTRODUCTION

Unsteady magnetohydrodynamic (MHD) boundary layer flows continue to stimulate significant interest in engineering sciences and applied physics owing to new emerging applications in magnetic materials processing [1], optimization of Hall and Faraday MHD generators [2], heat transfer control in nuclear reactors [3] and external ionized aerodynamics of flight vehicles [4]. The combined momentum, heat, and mass transfer from a vertical surface is particularly relevant to polymer processing dynamics [5] and also arises in electrochemical treatment of materials [6]. These flows may involve transverse static or alternating magnetic fields, oblique magnetic

fields, Hall currents, ionslip effects and Alfvén waves. They may also be laminar, transitional or turbulent in nature. The presence of diverse chemical reactions which are executed at different rates, in fluid mechanics processes in hydrometallurgy further necessitates mathematical modelling of thermal-mass diffusion processes including chemical reaction phenomena. Numerous transport processes feature combined buoyancy forces due to both thermal and mass diffusion in the presence of chemical reaction [7]. These processes are observed in chromatography, manipulation of materials, furnace combustion systems, solidification of binary alloys and crystal growth dispersion of dissolved materials, drying and dehydration operations in food processing plants, and rocket atomized liquid fuel burning. The presence of foreign mass in water or air may frequently generate some kind of chemical reaction. In many chemical engineering processes such as polymeric sheet extrusion, chemical reactions, which may be homogenous or heterogenous occur between a foreign mass and the fluid material which moves as a sheet. The interaction between homogeneous reactions in the bulk of fluid and heterogeneous reactions occurring on some catalytic surfaces is generally very complex, and this phenomenon may yield and also consume reactant species at different rates both within the fluid and on the catalytic surfaces as elaborated in detail by Aris [7]. Many simplified mathematical models of such processes (often termed *Sakiadis flows*) have been communicated. Das *et al.* [8] studied the influence of first-order homogeneous chemical reaction of unsteady flow from a vertical plate with the constant heat and mass transfer. Ferdows and Al Mdadall [9] investigated multiple order chemical reaction effects on coupled heat and mass transfer from an extending polymer sheet, observing that velocity, temperature and concentration are all reduced with increasing Schmidt number with fixed order of chemical reaction. They also noted that velocities are enhanced with greater order of reaction with constant Schmidt number and that concentrations are more strongly modified than temperatures with increasing order of chemical reaction. Makinde and Bég [10] employed Arrhenius chemical kinetics to examine inherent irreversibility and thermal stability in reactive magnetohydrodynamic isothermal channel flow, deriving solutions based on a perturbation method coupled with a special Hermite-Pade' approximation technique. They studied the velocity field, temperature field and thermal criticality conditions and computed volumetric entropy generation numbers, irreversibility distribution ratio and the Bejan number for the flow, demonstrating the sensitivity of stability to chemical reaction effects. Uddin *et al.* [11] studied magnetized reactive nanofluid flow numerically, noting that the flow is accelerated and temperatures increased while nanoparticle volume fraction is suppressed with increasing order of chemical reaction. Rao *et al.* [12] examined the chemical reaction effects on transient magneto-convection in porous media with heat generation. Zueco *et al.* [13] used an electrothermal network method and the PSPICE

software to analyse double-diffusive reactive convection from a buried cylinder in geological material. Mukhopadhyay *et al.* [14] examined transport of a species (solute), undergoing a chemical reaction, between a moving surface and a moving stream, showing that concentration boundary layer thickness is reduced with greater Schmidt number and reaction rate parameter, and mass absorption at the plate arises with a constructive chemical reaction. Makinde *et al.* [15] studied variable viscosity effects on a radially stretching nanofluid surface. Siddheshwar and Manjunath [16] investigated the effects of heterogeneous chemical reaction on the exchange, convective and diffusive coefficients in transient dispersion in a micropolar tube flow, showing that first coefficient arises due to the catalytic wall reaction which also modifies the other two coefficients.

Unsteadiness is also an important in coupled thermal and species diffusion problems. Time can have a significant influence on evolution of concentration and temperature profiles in boundary layer flows. Representative investigations of transient convective heat and mass transfer include Ruckenstein [17], Chang *et al.* [18] employed a local non-similarity method to study unsteady species diffusion in non-Newtonian boundary layer flows along a porous sheet. Unsteady nanofluid flow from a rotating stretching polymer sheet has been analyzed using a finite element method by Rana *et al.* [19]. Further studies of time-dependent diffusive boundary layer flows include Hussanan *et al.* [20] who considered unsteady magnetic convection in permeable materials with special thermal boundary conditions.

The above studies have neglected so-called “cross diffusion” effects. When heat and mass transfer occur simultaneously driving potentials between the fluxes can be of a more intricate nature. An energy flux can be generated not only by temperature gradients but by composition (species diffusion) gradients. The energy flux caused by a composition is called the Dufour or diffusion-thermo effect. Temperature gradients can likewise also create mass fluxes, and this is termed the Soret or thermal-diffusion effect. Generally, the thermal-diffusion and the diffusion thermo effects are of smaller-order magnitude than the effects prescribed by Fourier’s or Fick’s laws and are often neglected in heat and mass transfer processes. The thermal-diffusion effect, for instance, has been utilized for isotope separation and in mixing between gases with very light molecular weight (Hydrogen, Helium etc) and of medium molecular weight (Nitrogen-air) the diffusion-thermo effect was found to be of a significant magnitude. A very good review of the fundamentals of Dufour-Soret convection is provided in Gebhart [21] albeit for non-magnetic scenarios. Boundary-layer flows in the presence of Soret, and Dufour effects and with mixed convection have been addressed by several authors both with and without magnetic fields. Islam and Alam [22] investigated Dufour and Soret effects on transient hydromagnetic convection heat

and mass transfer flow in rotating porous media. Mansour *et al.* [23] obtained shooting solutions for reactive cross-diffusion magnetized boundary layer flow in thermally-stratified porous media. Prasad *et al.* [24] obtained numerical finite difference solutions for steady-state magnetohydrodynamic double-diffusive natural convection in non-Darcy porous media with Soret (thermo-diffusion) and Dufour (diffusion-thermo) effects included. They showed that increasing Soret number and simultaneously decreasing Dufour number boosts the local heat transfer rate (local Nusselt number) with the converse response computed for the mass transfer rate (local Sherwood number). Bég *et al.* [25] investigated Soret and Dufour effects on magneto-convection along an extending sheet embedded in a porous medium. Further examples of Soret-Dufour convection include Uwanta *et al.* [26] who examined magnetized Soret-Dufour flow from a vertical sheet under buoyancy forces. Bég *et al.* [27] studied Soret/Dufour effects on inclined plate solar panel convection.

Materials processing is frequently conducted at very high temperatures in which thermal radiation becomes significant. The interaction of buoyancy with thermal radiation is also often present in such processes and this permits the modification of flow fields and heat and mass transfer phenomena in order to produce specific characteristics in materials. Both isothermal and non-isothermal scenarios are relevant. Typical examples of materials fabrication applications include super alloy metallurgical liquid metal manufacturing [28], enclosure flows [29] and laser processing of magnetic materials [30]. Thermal radiation by its nature is intrinsically significantly more complex to simulate than conduction or convection. Not only is radiation a quartic temperature function, it also involves spectral effects, wavelength considerations, attenuation, sensitivity to geometrical characteristics and many other aspects. The general equation describing thermal radiation is also *integro-differential* in nature. For this reason it poses a formidable challenge for even numerical methods. Although numerous approaches have been developed for computing solutions to the radiative transfer equation including Chandrasekhar's discrete ordinates method [31] and Hamaker's 6-flux model [32], even these methods have their limitations and are computationally extremely intensive. They are also very difficult to implement for multi-physical flows where other body forces e.g. magnetic, gravity, surface tension etc, may be present and generally necessitate the use of commercial CFD (computational fluid dynamics) codes, which are not accessible to the vast majority of academic researchers. An alternative approach has been the use of the *algebraic flux approximation*. This methodology significantly simplifies radiative transfer problems by replacing the radiation intensity field with a differential formulation, usually of a 1-dimensional nature. While restricted to simpler systems, it does provide a reasonable estimate of radiative flux contribution and is

particularly appropriate for problems in which simultaneous convection and conduction heat transfer are present. Examples of this approach are the Traugott P1 differential approximation [33, 34], the Cogley-Vincenti-Giles non-gray flux approximation [35, 36], the Schuster-Schwartzchild dual flux approximation [37, 38] and the Rosseland-Boltzmann diffusion approximation [39, 40]. The last of these models is generally valid when the optical thickness of the medium in which radiation is propagating is very large (optically thick approximation). As optical thickness (optical depth) increases, thermal radiation is better attenuated in the medium and this induces heating. Optical thickness is a dimensionless quantification of how much a given medium retards the passage of thermal radiation. Radiative intensity falls by an exponential factor when optical thickness is unity. Physically, optical thickness will be a function of absorption coefficient, medium density and propagation distance. Modest [41] provides a succinct discussion of the applicability of the Rosseland-Boltzmann diffusion flux model. Cess [42] was probably the first researcher to implement this model in convective boundary layer flows, motivated by aerodynamics heating applications. Many studies have subsequently appeared deploying the Rosseland-Boltzmann model including Lee and Viskanta [43], Hossain and Rees [44], Uddin *et al.* [45], Ferdows *et al.* [46], Hayat *et al.* [47], Bég *et al.* [48], Sattar and Kalim [49] and Atdin and Kaya [50]. Several authors have also studied radiative convection flows in the presence of combined Soret and Dufour effects, including Shateyi *et al.* [51] who also considered magnetic field and Hall current effects in porous media and Olanrewaju and Gbadeyan [52] who investigated the collective influence of Soret/Dufour diffusive, chemical reaction, thermal radiation and volumetric heat generation/absorption effects on mixed convection stagnation point flows in permeable materials.

In this present work we conduct a numerical simulation of *radiative transient magnetohydrodynamic transport phenomena with chemical reaction from an impulsive-started vertical porous sheet*. Heat source/sink, Joule electromagnetic dissipation and viscous dissipation effects are included. A finite difference method (**FDM**) is employed based on Carnahan *et al.* [53]. Extensive validation of the FDM solutions is provided via a finite element method (**FEM**) based on the weak variational formulation [54]. Further validation is achieved with PSPICE-MAGNETO software employing the electro-thermal network simulation method (**NSM**) [55]. Recent relevant work in multi-physical materials processing has been communicated by Mabood *et al.* [56-58] describing various complex flows including magnetic stagnation flows with reaction, magnetized nanofluid stretching sheet flows and radiative non-Newtonian magnetic slip flows with chemical reaction. Further work has been presented by Mabood and Khan [59] on radiative-convective heat transfer in porous media using homotopy

analysis. All these studies justify further investigation into nonlinear heat and mass transfer in materials processing. In the present investigation, extensive interpretation of the effect of emerging thermophysical parameters on the heat, mass (species) diffusion and flow characteristics is documented. The study is relevant to high-temperature electromagnetic materials fabrication systems. To the authors' knowledge the present problem has not yet received the attention of the research community.

2. RADIATIVE MAGNETOHYDRODYNAMIC TRANSPORT MODEL

The physical regime under investigation is presented in **Fig. 1**. We consider transient magnetohydrodynamic (MHD) mixed convective heat and mass transfer in electrically-*conducting* incompressible viscous optically-dense flow from an electrically *non-conducting* isothermal permeable impulsive vertical sheet with thermal diffusion (Soret) and diffusion-thermo (Dufour) effects. The effects of internal heat generation, Joule heating (Ohmic magnetic dissipation) and viscous dissipation are incorporated. The applied magnetic field acts transversely to the sheet plane and is sufficiently weak to negate Hall current and other effects. The positive x -coordinate is measured along the sheet in the direction of fluid motion and the positive y -coordinate is measured normal to the sheet. Initially both the sheet and fluid are sustained at the same temperature $T(=T_\infty)$ and the same concentration level $C(=C_\infty)$. The fluid is stagnant and the sheet moves with a constant velocity U_∞ in its own plane. Instantaneously at time $t > 0$, the temperature of the plate and species concentration are raised to $T_w(>T_\infty)$ and $C_w(>C_\infty)$ respectively, which are thereafter sustained. Here, T_w, C_w are temperature and species concentration at the wall and T_∞, C_∞ designate the temperature and concentration of the species far from the wall (sheet) i.e. in the free stream, respectively. A uniform magnetic field \mathbf{H} is imposed parallel to the y -axis and it can be taken as $(0, H_0, 0)$. The magnetic Reynolds number is of sufficiently low value for induced magnetic field to be negligible in comparison with the applied magnetic field and therefore the magnetic lines are fixed relative to the fluid. Using the relation $\nabla \cdot \mathbf{J} = 0$ for the current density $\mathbf{J} = (J_x, J_y, J_z)$ where J_y is constant, since the sheet is non-conducting, $J_y = 0$ at the sheet and hence also vanishes everywhere. Assuming the sheet is infinite in extent, then all physical quantities are solely dependent on y and t . Unidirectional radiative flux (q_r) is assumed to act normal to the sheet. Incorporating the appropriate terms from the Maxwell electromagnetic field equations, following Takhar and Bég [60], with

the thermal Boussinesq approximation, the appropriate conservation partial differential equations including heat generation (or absorption) and chemical reaction terms, take the form:

Continuity equation;

$$\frac{\partial v}{\partial y} = 0 \quad (1)$$

Momentum equation;

$$\frac{\partial u}{\partial t} - v_0 \frac{\partial u}{\partial y} = \nu \frac{\partial^2 u}{\partial y^2} + gB_T(T - T_\infty) + gB_C(C - C_\infty) - \frac{\sigma \mu_e^2 H_0^2}{\rho} u \quad (2)$$

Energy (heat) equation;

$$\frac{\partial T}{\partial t} - v_0 \frac{\partial T}{\partial y} = \frac{\kappa}{\rho c_p} \frac{\partial^2 T}{\partial y^2} + \frac{Dk_t}{c_s c_p} \frac{\partial^2 C}{\partial y^2} + \frac{\nu}{c_p} \left(\frac{\partial u}{\partial y} \right)^2 + \frac{\sigma \mu_e^2 H_0^2}{\rho c_p} u^2 - \frac{1}{\rho c_p} \frac{\partial q_r}{\partial y} + \frac{Q}{\rho c_p} (T - T_\infty) \quad (3)$$

Concentration (species diffusion) equation;

$$\frac{\partial C}{\partial t} - v_0 \frac{\partial C}{\partial y} = D \frac{\partial^2 C}{\partial y^2} + \frac{Dk_t}{T_m} \frac{\partial^2 T}{\partial y^2} - k_0(C - C_\infty) \quad (4)$$

The corresponding initial and boundary conditions are;

$$t = 0; u=0, w=0, T = T_\infty, C=C_\infty \text{ everywhere}$$

$$t \geq 0; u = 0, w=0, T = T_\infty, C=C_\infty \text{ at } x=0$$

$$u = U_\infty, w=0, T = T_w, C = C_w \quad \text{at } y=0$$

$$u = 0, w=0, T \rightarrow T_\infty, C \rightarrow C_\infty \quad \text{as } y \rightarrow \infty \quad (5)$$

where u is the x component of velocity vector, v_0 is the transpiration (lateral wall mass flux) velocity, ν is the kinematic coefficient viscosity, μ is the fluid viscosity, ρ is the density of the fluid, κ is the thermal conductivity, c_p is the specific heat at the constant pressure, k_0 is the rate of chemical reaction and D is the coefficient of mass diffusivity, k_t is the thermal diffusion ratio, c_s is the concentration susceptibility, respectively. The radiative heat flux, q_r , is described by the Rosseland-Boltzmann approximation following Brewster [61]) such that

$$q_r = -\frac{4\sigma^*}{3k^*} \frac{\partial T^4}{\partial y}, \text{ where } \sigma^* \text{ and } k^* \text{ are the Stefan-Boltzman constant and the mean absorption}$$

coefficient, respectively. If the temperature differences within the flow is sufficiently small then T^4 can be expressed as a linear function after using Taylor series to expand T^4 about the free stream temperature T_∞ and neglecting higher-order terms. This results in the following approximation:

$$T^4 \approx 4T_\infty^3 T - 3T_\infty^4 . \quad (6)$$

To obtain the governing equations and the boundary condition in dimensionless form, the following non-dimensional quantities are introduced for transverse coordinate, velocity, time, temperature and concentration, respectively:

$$Y = \frac{yU_\infty}{\nu}, \quad U = \frac{u}{U_\infty}, \quad \tau = \frac{tU_\infty^2}{\nu}, \quad \bar{T} = \frac{T - T_\infty}{T_w - T_\infty} \quad \text{and} \quad \bar{C} = \frac{C - C_\infty}{C_w - C_\infty}. \quad (7)$$

Substituting the above dimensionless variables in equations (2)-(4) and corresponding boundary conditions (5) are:

Dimensionless Momentum;

$$\frac{\partial U}{\partial \tau} - S \frac{\partial U}{\partial Y} = \frac{\partial^2 U}{\partial Y^2} + G_r \bar{T} + G_c \bar{C} - MU \quad (8)$$

Dimensionless Energy equation;

$$\frac{\partial \bar{T}}{\partial \tau} - S \frac{\partial \bar{T}}{\partial Y} = \left(\frac{1+R}{P_r} \right) \frac{\partial^2 \bar{T}}{\partial Y^2} + D_u \frac{\partial^2 \bar{C}}{\partial Y^2} + E_c \left(\frac{\partial U}{\partial Y} \right)^2 + ME_c U^2 + \beta \bar{T} \quad (9)$$

Dimensionless Concentration;

$$\frac{\partial \bar{C}}{\partial \tau} - S \frac{\partial \bar{C}}{\partial Y} = \frac{1}{S_c} \frac{\partial^2 \bar{C}}{\partial Y^2} + S_r \frac{\partial^2 \bar{T}}{\partial Y^2} - \gamma \bar{C} \quad (10)$$

The corresponding normalized temporal and spatial initial and boundary conditions are transformed to:

$$\tau \leq 0; \quad U=0, \quad \bar{T} = 0, \quad \bar{C} = 0 \quad \text{everywhere}$$

$$\tau > 0; \quad U=0, \quad \bar{T} = 0, \quad \bar{C} = 0 \quad \text{at leading edge}$$

$$U = 1, \quad \bar{T} = 1, \quad \bar{C} = 1 \quad \text{at } Y = 0$$

$$U = 0, \quad \bar{T} = 0, \quad \bar{C} = 0 \quad \text{as } Y \rightarrow \infty \quad (11)$$

where τ represents the dimensionless time, Y is the dimensionless Cartesian coordinate, U is the dimensionless velocity, \bar{T} is the dimensionless temperature, \bar{C} is the dimensionless

concentration, $S = \frac{v_0}{U_\infty}$ (wall mass flux parameter; suction corresponds to $S > 0$ and injection to $S < 0$),

$G_r = \frac{gB_T(T_w - T_\infty)\nu}{U_\infty^3}$ (thermal Grashof number), $G_m = \frac{gB_C(C_w - C_\infty)\nu}{U_\infty^3}$ (species Grashof

number), $M = \frac{\sigma\mu_e^2 H_0^2 \nu}{\rho U_\infty^2}$ (magneto-hydrodynamic body force parameter), $R = \frac{16\sigma^* T_\infty^3}{3k^* \kappa}$

(Rosseland-Boltzmann conduction-radiation number), $P_r = \frac{\rho c_p \nu}{\kappa}$ (Prandtl Number),

$D_u = \frac{Dk_t}{\nu c_s c_p} \frac{(C_w - C_\infty)}{(T_w - T_\infty)}$ (Dufour diffuso-thermal number), $E_c = \frac{U_\infty^2}{c_p(T_w - T_\infty)}$ (Eckert Number),

$\beta = \frac{Q\nu}{\rho c_p U_\infty^2}$ (heat generation/absorption parameter), $S_c = \frac{\nu}{D}$ (Schmidt Number),

$S_r = \frac{Dk_T}{\nu T_m} \frac{(T_w - T_\infty)}{(C_w - C_\infty)}$ (Soret thermo-diffusion number) and $\gamma = \frac{k_0 \nu}{U_\infty^2}$ (chemical reaction

parameter). The quantities of chief physical interest are the wall shear stress, Nusselt number (surface heat transfer rate) and Sherwood number (surface mass transfer rate). Shear stress at the

sheet, $\tau_x = \mu_0 \left(\frac{\partial u}{\partial y} \right)_{y=0}$ which is associated with $\left(\frac{\partial U}{\partial Y} \right)_{Y=0}$. From the temperature field, the

effects of various parameters on the heat transfer coefficients can be analyzed. The Nusselt

number, $N_u = -\mu_0 \left(\frac{\partial T}{\partial y} \right)_{y=0}$ is associated with $-\left(\frac{\partial \bar{T}}{\partial Y} \right)_{Y=0}$. From the concentration field, the

effects of various parameters on the local and average mass transfer coefficients can be studied.

The mass transfer rate is quantified via the well-known Sherwood number, $S_h = -\mu_0 \left(\frac{\partial C}{\partial y} \right)_{y=0}$

which is linked to $-\left(\frac{\partial \bar{C}}{\partial Y} \right)_{Y=0}$.

3. FINITE DIFFERENCE NUMERICAL SOLUTIONS

To solve the non-dimensional system defined by eqns. (8)-(10) under boundary conditions (11), we employ an implicit finite difference method (FDM). Following Carnahan *et al.* [53], the dimensionless partial differential equations are formulated as a set of *finite difference* equations.

The boundary layer domain is discretized as depicted in **Fig. 2**. Let $U^{\bar{n}}$, $T^{\bar{n}}$ and $C^{\bar{n}}$ denote the

values of U , \bar{T} and \bar{C} at the end of a time-step respectively. Using the implicit finite difference approximation, the following appropriate set of finite difference equations are generated:

Momentum:

$$\frac{U_k^{\bar{n}+1} - U_k^{\bar{n}}}{\Delta\tau} - S \frac{U_{k+1}^{\bar{n}} - U_k^{\bar{n}}}{\Delta Y} = \frac{U_{k+1}^{\bar{n}} - 2U_k^{\bar{n}} + U_{k-1}^{\bar{n}}}{(\Delta Y)^2} + G_r \bar{T}_k^{\bar{n}} + G_m \bar{C}_k^{\bar{n}} - MU_k^{\bar{n}} \quad (12)$$

Heat (Energy):

$$\begin{aligned} \frac{\bar{T}_k^{\bar{n}+1} - \bar{T}_k^{\bar{n}}}{\Delta\tau} - S \frac{\bar{T}_{k+1}^{\bar{n}} - \bar{T}_k^{\bar{n}}}{\Delta Y} = & \left(\frac{1+R}{P_r} \right) \frac{\bar{T}_{k+1}^{\bar{n}} - 2\bar{T}_k^{\bar{n}} + \bar{T}_{k-1}^{\bar{n}}}{(\Delta Y)^2} + D_u \frac{\bar{C}_{k+1}^{\bar{n}} - 2\bar{C}_k^{\bar{n}} + \bar{C}_{k-1}^{\bar{n}}}{(\Delta Y)^2} \\ & + E_c \left(\frac{U_{k+1}^{\bar{n}} - U_k^{\bar{n}}}{\Delta Y} \right)^2 + ME_c (U_k^{\bar{n}})^2 + \beta (\bar{T}_k^{\bar{n}}) \end{aligned} \quad (13)$$

Concentration (Species Diffusion)

$$\frac{\bar{C}_k^{\bar{n}+1} - \bar{C}_k^{\bar{n}}}{\Delta\tau} - S \frac{\bar{C}_{k+1}^{\bar{n}} - \bar{C}_k^{\bar{n}}}{\Delta Y} = \frac{1}{S_c} \frac{\bar{C}_{k+1}^{\bar{n}} - 2\bar{C}_k^{\bar{n}} + \bar{C}_{k-1}^{\bar{n}}}{(\Delta Y)^2} + S_r \frac{\bar{T}_{k+1}^{\bar{n}} - 2\bar{T}_k^{\bar{n}} + \bar{T}_{k-1}^{\bar{n}}}{(\Delta Y)^2} - \gamma (\bar{C}_k^{\bar{n}}) \quad (14)$$

The associated spatial boundary conditions are:

$$U_0^{\bar{n}} = 1, \bar{T}_0^{\bar{n}} = 1, \bar{C}_0^{\bar{n}} = 1 \quad (15)$$

$$U_L^{\bar{n}} = 0, \bar{T}_L^{\bar{n}} = 0, \bar{C}_L^{\bar{n}} = 0 \text{ where } L \rightarrow \infty \quad (16)$$

Here the subscript k designates the grid points with Y coordinate and the superscript \bar{n} represents a value of time, $\tau = \bar{n}\Delta\tau$ where $\bar{n} = 0, 1, 2, \dots$. The velocity (U), temperature (\bar{T}) and concentration (\bar{C}) distributions at all interior nodal points may be computed by successive applications of the above finite difference equations. The numerical values of the shear stress, Nusselt number and Sherwood number are evaluated by **five-point** approximate

formula for the derivatives. The stability conditions are $M \frac{\Delta\tau}{2} + S \frac{\Delta\tau}{\Delta Y} + \frac{2\Delta\tau}{(\Delta Y)^2} \leq 1$,

$$-\beta \frac{\Delta\tau}{2} + S \frac{\Delta\tau}{\Delta Y} + \left(\frac{1+R}{P_r} \right) \frac{2\Delta\tau}{(\Delta Y)^2} \leq 1 \quad \text{and} \quad \gamma \frac{\Delta\tau}{2} + S \frac{\Delta\tau}{\Delta Y} + \frac{1}{S_c} \frac{2\Delta\tau}{(\Delta Y)^2} \leq 1. \quad \text{When } \Delta\tau \text{ and } \Delta Y$$

approach zero then numerical convergence is achieved i.e. the computational results of the implicit finite difference method approach the actual solutions.

4. VALIDATION WITH FINITE ELEMENT METHOD (FEM)

The **FDM** numerical solutions have been validated using a Galerkin finite element method (**FEM**) based on the variational (weak) formulation, as elaborated in detail in Rao [62]. This approach has been used extensively in recent years in transient and magnetohydrodynamic (MHD) flows. For example Gupta *et al.* [63] studied non-Newtonian heat transfer from an extending polymer sheet at high temperature with FEM. Other applications which have successfully simulated complex nonlinear flow problems with FEM algorithms include pulsatile magneto-hemodynamics [64], magnetized micro-continuum polymer flow [65], oscillatory conducting nanofluid dynamics from circular bodies (spacecraft) [66] and solar collector nano-convection [67]. FEM uses the opposite approach to FDM, viz numerical integration rather than numerical differentiation, which is infact much more efficient computationally. Applying the Galerkin finite element method to equations (8) to (10) over the element (e) ($y_j \leq y \leq y_k$), we have following Bég *et al.* [64]:

Finite element momentum equation:

$$\int_{y_j}^{y_k} N^{(e)T} \left(\frac{\partial U^{(e)}}{\partial \tau} - S \frac{\partial U^{(e)}}{\partial Y} - \frac{\partial^2 U^{(e)}}{\partial Y^2} - G_r \bar{T} - G_r \bar{C} + MU^{(e)} \right) dy = 0 \quad (17)$$

Finite element energy equation;

$$\int_{y_i}^{y_k} N^{(e)T} \left[\frac{\partial \bar{T}^{(e)}}{\partial \tau} - S \frac{\partial \bar{T}^{(e)}}{\partial Y} - \left(\frac{1+R}{P_r} \right) \frac{\partial^2 \bar{T}^{(e)}}{\partial Y^2} - D_u \frac{\partial^2 \bar{C}}{\partial Y^2} - E_c \left(\frac{\partial U}{\partial Y} \right)^2 - ME_c U^2 - \beta \bar{T}^{(e)} \right] dy = 0 \quad (18)$$

Finite element concentration equation;

$$\int_{y_i}^{y_k} N^{(e)T} \left[\frac{\partial \bar{C}^{(e)}}{\partial \tau} - S \frac{\partial \bar{C}^{(e)}}{\partial Y} - \frac{1}{S_c} \frac{\partial^2 \bar{C}^{(e)}}{\partial Y^2} - S_r \frac{\partial^2 \bar{T}}{\partial Y^2} + \gamma \bar{C}^{(e)} \right] = 0 \quad (19)$$

Next, we postulate *linear piecewise approximate* solutions for the velocity, temperature and concentration functions with appropriate shape functions (interpolation functions). In order to prove the convergence and stability of the Galerkin finite element method, the **Matlab** program **MAGNETO-FEM** is executed with slightly modified values of the mesh distance in the *y*-and τ -directions *i.e.* *j* and *k*, and no significant change is observed in the values of the velocity components. Mesh independence of solutions was therefore achieved with excellent stability and convergence. The boundary conditions (10) are easily specified in **MAGNETO-FEM**. To validate the **FDM** finite difference code, a comparison solution is performed for each of the

plots in Section 6 i.e. **Figs 4a,b-13a,b**. For all cases, excellent correlation is achieved between **FDM** and Galerkin **MAGNETO-FEM**. The boundary layer regime is discretized into a domain which is delineated into smaller elements (sub-domains) of finite dimensions called “finite elements”. The collection of elements is called *the finite-element mesh* or grid. The element matrix, which is called a *stiffness matrix*, is constructed by using *element interpolation functions*. The algebraic equations so obtained are assembled by imposing the inter-element continuity conditions. This yields a large number of algebraic equations defining the *global finite element model*, which governs the whole domain. The essential and natural boundary conditions are imposed on the assembled equations. The assembled equations so obtained can be solved by any “matrix” numerical technique e.g. Householder’s approach, LU Decomposition method, Choleski decomposition etc. Further details are readily available in [63-67]. Criteria for the selection for elements are also documented in [63-67]. The non-linear algebraic system of equations is solved iteratively. An accuracy of 0.00001 is used. A convergence criterion based on the relative difference between the current and previous iterations is employed. When these differences reach the desired accuracy, the solution is assumed to have converged and the iterative process is terminated. Two-point Gaussian quadrature is implemented for solving the integrations. The FEM algorithm has been executed in **MATLAB** running on an Octane SGI desktop workstation and takes 15-20 seconds on average. We note that in **Figs. 4a,b-13a,b** the green triangles () denote the **MAGNETO-FEM** solutions. Confidence in the **FDM** code is therefore justifiably high. However to further validate the solutions, in the absence of results from other studies and to provide a rigorous benchmark for future simulations, we have also verified the FDM and FEM computations with a network method which is described briefly next.

5. FURTHER VERIFICATION WITH NETWORK SIMULATION METHOD

The transformed partial differential equations (8) to (10) subject to the temporal and spatial boundary conditions (11) have been solved with the MAG-PSPICE Network Simulation Method software (**NSM**) approach. This technique is founded on the *thermo-electrical analogy* and has been implemented in many diverse areas of applied mechanics, thermal sciences and fluid dynamics, being equally adept at solving linear and non-linear, steady or transient, hydrodynamic or coupled transport problems. Network simulation methodology uses the network theory of thermodynamics, in which flux-force relationships in dynamical systems are modelled using electric networks. NSM effectively exploits the formal similarities

between the mathematical structure underlying different phenomena with the same balance and constitutive equations and intrinsic to this approach is the design of an “analogous electric circuit” which possesses the same balance and constitutive equations as the physical problem of interest. **NSM** was introduced by Nagel [68] originally for semiconductor and transient electrical circuit problems. It has more recently been implemented in magnetic tribology (squeeze films for spacecraft landing gear) [69], magnetic biopolymer materials processing [70], magneto/electro-rheological (M/ER) smart lubrication [71] systems for earthquake shock protection (seismic bearings) and electro-kinetic stabilization of geotechnical materials [72]. Discretization of the *differential* equations is founded on the *finite-difference methodology*, where only a discretization of the spatial co-ordinates is necessary. Numerical differentiation is implicit in such methods and some expertise is required in avoiding numerical diffusion, instability and convergence problems. **NSM** simulates the *electrical variable of voltage* as being equivalent to the velocity (U), temperature (\bar{T}) and concentration (\bar{C}), while the *electrical current* is equivalent to the velocity flux ($\partial U/\partial Y$), temperature flux ($\partial \bar{T}/\partial Y$) and concentration flux ($\partial \bar{C}/\partial Y$). A network electrical model for *each* volume element is designed so that its electrical equations are formally equivalent to the spatial discretized equation. The whole network model, including the devices associated with the boundary conditions, is solved by the modified numerical computer code **Pspice** [69]. *Fourier’s* law is utilized in the spatial discretization of the dimensionless transport equations. The electrical analogy is applied to the discretized equations together with *Kirchhoff’s* law for electrical currents. To implement the boundary conditions, constant voltage sources are employed for velocity, temperature and concentration. *Time* remains as a real continuous variable. Researchers need not manipulate the finite difference differential equations to be solved nor expend effort in convergence exercises. The principal advantage of **NSM** is that it negates the requirement in standard numerical finite difference schemes of manipulation of difference equations and the constraints of specified yardsticks around the convergence of numerical solutions. Details of the discretization and electronic network diagram construction have been provided in many previous studies and the reader is referred to Zueco and Bég [69] and Bég and Bég [71, 72]. The **MAG-SPICE** code is designated the “electric circuit simulator”. Nagel [68] has elucidated in detail the local truncation errors present in the original **SPICE** algorithm. A necessary criterion for using **MAG-SPICE** effectively is a familiarity with electrical circuit theory. Momentum, temperature and concentration balance “currents” are defined systematically for each of the discretized equations and errors can be quantified in terms of the quantity of control volumes. The user however needs to program

a customized protocol file, (file “*MagNetwork.cir*”). This program rapidly generates the file for execution in MAG-PSPICE, and the program permits the reading of the solutions provided by MAG-PSPICE (file “*MagNetwork.out*”). Following the simulations, the code plots waveform results so the designer can visualize circuit behavior and determine design validity. Graphical results of each simulation are presented in the MAG-PSPICE “Probe window waveform viewer” and analyzer, where it is possible to see the velocity, temperature and concentration field at any point of the boundary layer. A summary of the procedure is given in **Fig. 3** below. NSM implements the most recent advances in software in the resolution of electrical networks to solve diverse types of partial differential equations which may be elliptical, hyperbolic, parabolic, linear, non-linear and 1-, 2- or 3-dimensional. At least one of the FDM and FEM computations in each of the **Figs. 4a,b-13a,b** have been closely verified with MAG-PSPICE. The NSM (MAG-PSPICE) solutions are given as red diamonds (◆). The FDM computations are therefore shown to be highly accurate as corroborated by two independent numerical simulation tools. Although steady-state models do exist with which we can benchmark very special reduced cases of the general model presented in the current article, we have opted to validate the general model including all thermophysical effects i.e. Ohmic dissipation, Soret and Dufour effects and also chemical reaction. This is a significantly more zealous approach and confirms all possible families of solutions obtained by the FDM code with the two other codes. Moreover, it provides extensive confidence to other researchers who may wish to extend the present model to for example non-Newtonian flow and are therefore provided with extensive graphical solutions to validate their own programs. In all three numerical methods, we have adopted data from a number of references to achieve physically viable simulations. These include refs. [23], [44] and [51] which cover all the essential parameters featured in the present model. Furthermore we have used the references [61, 73] for additional guidance as to parameter selection.

6. FDM COMPUTATIONAL RESULTS AND DISCUSSION

Extensive FDM simulations have been conducted and are illustrated in **Figs. 4a,b-13a,b**. In order to investigate the transport phenomena characteristics inherent to the current radiative magnetic materials processing problem, numerical results are depicted graphically for velocity (U), temperature (\bar{T}) and concentration (\bar{C}) versus transverse coordinate. Furthermore transient plots for shear stress, Nusselt number and Sherwood number are included. The

influence of wall mass flux parameter (S), magnetic body force parameter (M), Rosseland-Boltzmann conduction-radiation parameter (R), Prandtl number (P_r), Dufour number (D_u), Eckert number (E_c), heat sink/source parameter (β), Schmidt number (S_c), Soret number (S_r), and chemical reaction parameter (γ) on the different transport characteristics is studied and visualized with the help of a computer programming language Compaq Visual Fortran 6.6a. **Tecplot 7** was deployed to visualize the FDM numerical results. To obtain the steady-state solutions, the computations have been carried out up to dimensionless time, $\tau = 80$. It is observed that the numerical values of U , \bar{T} and \bar{C} however, show no tangible changes after $\tau = 15$. Hence at $\tau = 15$ the solutions of all variables are taken to have converged to *steady-state* solutions. For the sake of brevity although every parameter arising in the transport model is studied, we confine the examination of parameter effects on selected variables. We further emphasize that for every plot depicted *at least one* FDM solution has been validated with the FEM (green triangles) and NSM (red diamond) numerical codes. Furthermore we have conducted mesh independence (grid tests) with the codes. Grid independence is usually essential to show if only one numerical scheme is used. We have used three. The solutions have all been shown to agree between FEM, network simulation and finite difference methods. The grids used were obviously successively refined to achieve the correct converged solution. Table 1 provides the mesh independence for the three different numerical methods utilized. This has been done, for one variable i.e. the steady state velocity solution (U), with all thermo-physical parameters also given. Generally all the methods used achieve mesh independence with 100 steps in the Y -direction, for the steady state solution. Further improvement in the solution is not required after this stage and it is assumed that the solution has converged. To determine the physical influence of the key thermophysical effects, we have presented *steady-state* solutions in **Figs. 4a,b-10a,b** and *time-dependent* solutions in **Figs 11a,b-13a,b**.

Figs 4a,b-6a,b illustrate the evolution in velocity profiles for various values of wall mass flux parameter (S), magnetic parameter (M), conduction-radiation parameter (R), Dufour number (D_u), Prandtl number (P_r), heat generation/absorption parameter (β), Eckert number (E_c) and Soret number (S_r). The case of $\beta < 0$ and $\beta > 0$ are treated respectively as heat absorption and generation and correspond to “hot sink” and “hot spot” scenarios in materials processing. In fig 4a excellent correlation is achieved for the case of $S = 2.00$ with all three numerical codes i.e. **FDM**, **FEM** and **NSM**. With increasing S values which imply progressively greater suction (lateral mass flux removal via the permeable sheet from the boundary layer flow), there is a significant deceleration in the boundary layer flow i.e. velocity magnitudes are depressed.

Values are however consistently positive demonstrating that flow reversal is never induced. The monotonic decay in velocity profiles for any suction value is smoothly computed from the permeable sheet (wall) into the free stream. The asymptotic tendency of profiles indicates and confirms the imposition of an adequately large “infinity boundary condition” and verifies that indeed correct solutions are achieved for the steady state. Greater suction essentially draws the momentum boundary layer closer to the sheet surface i.e. causes stronger adherence which serves to destroy momentum and delay boundary layer separation. An increase in magnetic body force parameter (M) is observed in fig. 4b, to substantially depress the velocity magnitudes, although once again (as with increasing suction) no back-flow is instigated in the boundary layer regime. The magnetic field effect is sustained via *a single linear body force term* in the

dimensionless momentum equation (8), namely $-MU$. $M(= \frac{\sigma \mu_e^2 H_0^2 \nu}{\rho U_\infty^2})$ represents the relative

influence of the *Lorentzian magneto-hydrodynamic body force* (acting transverse to the direction of the applied magnetic field i.e. in the Y - direction) to the *inertial force*. For increasing values of M , the Lorentzian body force, which is a drag force, becomes stronger and this impedes the flow. The flow is therefore strongest with weak magnetic field ($M = 3.00$) and most inhibited with strongest magnetic field ($M=15.0$). In Fig. 5a, six sets of three profiles are plotted to study the collective influence of conduction-radiation parameter (R) and Dufour number (Du). Each cluster of triple profiles corresponds to a single Du value and three R values. With an increase in Dufour number, there is a significant enhancement in velocity. Dufour number,

$D_u = \frac{Dk_t}{\nu c_s c_p} \frac{(C_w - C_\infty)}{(T_w - T_\infty)}$, embodies the ratio of the increase in enthalpy of a unit mass during

isothermal mass transfer divided by the enthalpy of a unit mass of mixture. It arises in the second order cross-diffusion gradient term, in the normalized energy equation (9), $D_u \frac{\partial^2 \bar{C}}{\partial Y^2}$.

Effectively it simulates the influence of species diffusion on the thermal diffusion field (temperature). The Dufour effect is the reciprocal phenomenon of the Soret effect. The latter (thermal diffusion) represents the occurrence of a diffusion flux due to a temperature gradient whereas the former is the occurrence of a heat flux due to a chemical potential gradient. Dursunkaya and Worek [73] have also identified the accelerating effect of Dufour number on boundary layer flows. Their analysis confirms the present trend, namely that flow velocity is minimized with absence of the Dufour effect (curves 1). The presence of strong heat flux induced by the species diffusion aids momentum diffusion and accelerates the flow. The influence of Rosseland-Boltzmann (conduction-radiation) number (R) on velocity evolution is

also interesting. This parameter arises in the augmented thermal diffusion term also in the energy conservation eqn. (9), viz $\left(\frac{1+R}{Pr}\right)\frac{\partial^2\bar{T}}{\partial Y^2} \cdot R = \frac{16\sigma^*T_\infty^3}{3k^*\kappa}$ which simulates the relative role of thermal *radiative* heat transfer compared with thermal *conduction* heat transfer. As R is increased thermal radiation contributes more and this elevates the heat flux in the medium which aids in accelerating the flow. A similar observation has been reported by numerous other studies including Hossain and Rees [44], Hayat *et al.* [47] and Sattar and Kalim [49], although they have not explained the cause for flow acceleration. Increasing thermal radiation implies that the random kinetic energy of charged particles is elevated. This *energizes* the boundary layer and boosts heat flux leading to a momentum enhancement which accelerates the flow. Evidently the velocity of the fluid is minimized for low values of R (0.05) and peaks for highest value of R (0.15). The influence is non-trivial. Smooth convergence of all profiles is attained in the free stream again testifying to the imposition of an adequately large infinity boundary condition ($Y=6$) in the computations. In fig. 5b an increase in Prandtl number (Pr) is clearly seen to decrease velocities. Prandtl number defines the ratio of viscous diffusion to thermal diffusion in the boundary layer regime. For $Pr > 1$, momentum diffusivity will exceed thermal diffusivity, whereas for $Pr < 1$ thermal diffusivity will exceed momentum diffusivity. With greater Pr , since the velocity is reduced, there is a corresponding increase in momentum boundary layer thickness. The presence of a heat source ($\beta = 0.5$) is found to accelerate the flow at low Pr (0.71), whereas a heat sink ($\beta = -0.5$) induces the opposite effect and depresses the flow velocity. There is no tangible modification in flow velocity with either heat sink (absorption) or heat source (generation) at high Pr (7.0). $\beta\bar{T}$ is the heat source/sink term appearing in the energy eqn. (9) as a linear temperature term. The effect is straightforward and has been documented by many researchers, notably Stewart and Burns [74] where a similar observation has been reported to that of the present computations. Fig. 6a reveals that with increasing Eckert number (Ec) a significant elevation in flow velocity is generated. Conventional viscous dissipation, which is associated with the Eckert number, appears in the energy eqn. (9) as the familiar quadratic spatial velocity gradient, viz, $Ec\left(\frac{\partial U}{\partial Y}\right)^2$. However since magnetic field is non-zero ($M=3.0$) the Ohmic dissipation (Joule heating) term is also invoked which is a product of magnetic parameter, Eckert number and square of the velocity, ME_cU^2 . The kinetic energy of the fluid is enhanced with greater Ec values. This is observed in a strong acceleration in the flow. Free convection currents also arise for $Ec > 0$ and these aid in accelerating the flow in the boundary layer. The converse would arise for $Ec < 0$ although this

case is not considered here. Schlichting [75] defines Eckert number as representing the ratio of kinetic energy at the wall to the specific enthalpy difference between wall and fluid i.e. quantifying frictional heat due to mechanical dissipation effects internal to the fluid. It is therefore intimately associated with dissipation created by shear stresses in the fluid at the wall. Dissipation takes place mainly where the greatest velocity gradients are and this location is not situated at the wall where the fluid adheres, but in the boundary layer. Gebhart [76] demonstrated very early that positive Eckert number leads to boundary layer acceleration. Gebhart and Mollendorf [77] further confirmed this trend. The present results would therefore appear to be consistent with other investigations. Fig. 6b indicates that a rise in Soret number (S_r) substantially boosts the velocity. This effect which is also variously referred to as the thermophoretic effect is common in mixtures of mobile particles where the different particle types exhibit different responses to the force of a temperature gradient. S_r arises in the second order temperature gradient in the species diffusion eqn. (10), viz $S_r \frac{\partial^2 \bar{T}}{\partial Y^2}$, and evidently exerts a marked influence on velocity, since molecular diffusion encourages momentum diffusion. Diffusion of matter caused by temperature gradients (Soret Effect) and diffusion of heat caused by concentration gradients (Dufour Effect) become significant when temperature and concentration gradients are very large, as considered in the present study. Generally these effects are considered as a *second order* phenomenon but can exert first order effects. Weaver and Viskanta [78] have reported similar findings to those in fig. 6b, namely that when the differences of the temperature and the concentration are large or when the difference of the molecular mass of the two elements in a binary mixture is great, the coupled interaction is significant enough to aid momentum development in buoyancy-driven convection. In figs 5a, b-6a, b again excellent correlation is achieved with FDM, FEM and NSM numerical techniques.

Figs. 7a,b, 8a,b and 9a illustrate the temperature (\bar{T}) response to various thermophysical parameters. Increasing suction ($S > 0$) in fig. 7a is observed to strongly suppress temperatures throughout the boundary layer. A velocity overshoot is also witnessed in close proximity to the wall, and this is amplified with stronger suction effect. Fig. 7b shows that greater magnetic parameter (M) enhances temperatures throughout the regime from the wall to the free stream. The additional work which must be carried out by the fluid in dragging itself against the imposed magnetic field is dissipated as thermal energy. This results in heating of the fluid and an increase in thermal boundary layer thickness. The effect is prominent and is a classical result in magnetohydrodynamic convection, as identified in many other studies. The pertinence to materials processing is that supplementary heat can be produced with transverse static magnetic

fields, to aid in the manipulation of materials which when combined with thermal radiative flux and heat generation, provides engineers with a powerful combination for thermally-induced modification of materials. Fig. 8a shows that the temperatures are enhanced generally with increasing Rosseland-Boltzmann number (R) and also with greater Dufour number (Du). As elaborated earlier the parameter, R represents the relative contribution of radiative to conduction heat transfer. It arises in the augmented thermal diffusive flux term. As this parameter is increased, progressively stronger radiative flux is present which energizes the flow and elevates temperatures and also thermal boundary layer thickness.

Similarly the Dufour number which encapsulates the contribution of species concentration gradients to the thermal field successfully aids in heating the regime and also elevating thermal boundary layer thickness. Peak temperatures generally arise close to the sheet and they are systematically displaced further from the sheet with increasing R and Du values. Thermal boundary layer thickness is effectively increased with greater radiative flux and also diffusothermal (Dufour) cross-diffusion effects. In all cases, temperature profiles follow a smooth decay from the wall to the free stream indicating that the FDM (and where appropriate the MAGNETO-FEM and MAG-SPICE NSM) computational solutions are stable and convergent with an adequate infinity (free stream) boundary condition prescribed in each respective numerical code. Fig 8b illustrates the response of temperature function to a variation in both Prandtl number and heat source/sink parameter. It is apparent that increasing Prandtl number (Pr) significantly depresses temperatures in the boundary layer. Prandtl number signifies the ratio of momentum diffusivity to thermal diffusivity. It is the single most important parameter in heat transfer analysis since it corresponds to actual physical properties of fluids unlike the vast majority of other dimensionless thermofluid numbers. Higher Prandtl values imply a thinner thermal boundary layer thickness and more uniform temperature distributions across the boundary layer. Hence the thermal boundary layer will be much reduced in thickness compared with the hydrodynamic (momentum) boundary layer. Prandtl number < 1 corresponds to greater thermal diffusion rate compared with momentum diffusion rate. A lower Prandtl number ($Pr = 0.71$ i.e. gas) implies that the fluid will possess *higher thermal conductivity* (and an associated thicker thermal boundary layer structure) so that heat can diffuse away from the vertical surface faster than for higher Prandtl number fluid ($Pr = 7.0$ i.e. liquids associated with thinner boundary layers). Therefore lower Prandtl number fluids will achieve significantly larger temperatures in the boundary layer. Higher Prandtl number fluids possess lower thermal conductivities causing less thermal energy to be diffused from the sheet surface into the body of the fluid and resulting in lower temperatures. With heat generation (source) i.e. $\beta=0.5$, temperatures are, as expected,

increased, whereas with heat absorption (sink) i.e. $\beta = -0.5$ temperatures are depressed. The case where no heat sink/source is present i.e. $\beta = 0$, naturally falls between the other two cases. Fig. 9a presents the evolution of the temperature with a variation in the dissipation parameter, Ec . As anticipated the increase in viscous dissipation manifests with an addition of thermal energy to the flow which results in a rise in temperature. Thermal boundary layer thickness is also enhanced. Temperature overshoot is present in the vicinity of the wall and this has also been observed in numerous other investigations including Gebhart [76]- it is a characteristic feature of double-diffusive convection flows. The temperature overshoot migrates further from the wall (sheet) with greater Eckert number. Temperature profiles converge towards each other in the free stream.

Figs. 9b and 10 a, b depict the spatial species concentration evolution with various emerging parameters. In fig. 9b, the influence of the lateral wall mass flux i.e. suction parameter, S , is shown. This simple parameter is associated with geometric modification of the sheet (wall) via perforations. It arises not only in the dimensionless momentum eqn. (8) in the linear velocity gradient term, but also in the heat eqn. (9) and concentration eqn. (10) where it is coupled with the linear temperature gradient $(-S \frac{\partial T}{\partial Y})$ and linear concentration gradient $(-S \frac{\partial \bar{C}}{\partial Y})$ terms, respectively. Concentration clearly decreases with increasing suction effect i.e. removal of the fluid (not species) via the sheet. The destruction in momentum associated with greater suction forces the boundary layer to adhere more strongly to the wall and this discourages species diffusion. In Fig. 10a, the species concentration profiles for several values of chemical reaction parameter (γ) with two values of Schmidt number $Sc = 0.60$ (water vapor) and $Sc = 0.94$ (carbon dioxide) are presented, respectively. It is noted that the concentration decreases with the increase of chemical reaction parameter (γ), where $\gamma < 0$ and $\gamma > 0$ are treated as generative and destructive chemical reactions respectively. The appropriate term in the concentration eqn. (10) is the linear term, $-\gamma \bar{C}$. With increasingly negative γ values more species is converted via chemical reaction and this boosts the species concentration levels in the boundary layer. With increasingly positive γ - values the opposite effect is induced, namely, less species is converted and this manifests in a reduction in concentration levels. Similar findings have been documented by Chaudhary and Merkin [79] among others. Schmidt number (Sc) embodies the ratio of the mass (species) and viscous diffusion time scales. It also defines the ratio of momentum diffusivity to species diffusivity. The Schmidt number in mass transfer is analogous in importance to the Prandtl number in heat transfer, as both are associated with properties of fluids and diffusing species, respectively. For $Sc < 1$ (as considered in the present materials

processing problem), the momentum diffusivity is lower than the species (mass) diffusivity and the species diffusion rate exceeds the momentum diffusion rate. For $Sc > 1$ (not considered here) this scenario is reversed. Higher values of Sc correspond to higher density species diffusing in air, e.g. $Sc = 1.0$ corresponds to methanol diffusing in electrically conducting gas, $Sc = 2.0$ may represent ethyl-benzene diffusing in air. Here we are concerned with low molecular weight gas diffusion in denser liquids e.g. saline solutions, low viscosity electro-conductive polymeric materials etc. Schmidt numbers less than 1 are therefore appropriate. Increasing Sc lowers the *chemical molecular diffusivity* of the species. As Sc is increased the concentration boundary layer will become relatively thinner than the viscous (momentum) boundary layer. Concentrations will therefore be reduced and species boundary layer thickness will also be decreased. With thinner concentration boundary layers, the concentration gradients will be enhanced due to an inhibition of species flux in the boundary layer. For $Sc < 1$, species diffusivity exceeds momentum diffusivity and this accounts for the greater concentration values for $Sc = 0.64$ compared with the minimized concentration profile for $Sc = 0.94$. The implication for materials processing engineers is that in such a regime, a *lower Schmidt number* diffusing species must be employed to *enhance concentration* distributions in the medium which may then be manipulated to alter the magnetic material characteristics for different applications (aerospace, medical, energy etc). Fig. 10b demonstrates that a dual effect is induced by increasing Soret number. In the near -wall region, concentration of the species decreases within the interval $0 < Y < 0.45$ (approximately) with an increase in Soret number. However for $Y > 0.45$ the concentration magnitudes are markedly elevated with greater Soret number. Evidently there is therefore a critical distance from the wall (sheet) at which the Soret (thermo-diffusion) gradient, $S_r \frac{\partial^2 \bar{T}}{\partial Y^2}$, appearing in eqn. (10) terminates its opposing influence on species diffusion and commences an assisting role. Further detailed analysis is therefore required to elaborate the exact mechanism by which this phenomenon arises and will be addressed in a separate study. The asymptotic decay of concentration profiles towards the free stream, for any Soret number is clearly attained in Fig. 10b.

Figs. 11a,b-13a,b depict respectively the transient shear stress, Nusselt number and Sherwood number distributions at the sheet ($Y=0$) for variation in Eckert number (E_c), Soret number (S_r), Suction parameter (S), chemical reaction parameter (γ) and Schmidt number (Sc), with all other parameters constrained. Shear stress (τ_x) is clearly strongly enhanced with greater dissipation effect (Eckert number) as seen in fig. 11a. Generally shear stresses ascend very rapidly from the initiation of the flow and all attain the steady state distribution for $\tau = 15$.

Increasing Soret number (fig. 11b) is also observed to considerably elevate the shear stress values indicating significant acceleration in the boundary layer flow. Conversely with increasing Eckert number (fig. 12a), there is a substantial reduction in Nusselt number. The increase in thermal energy in the fluid with greater dissipation causes heat to diffuse more intensively from the boundary layer to the wall (sheet) leading to a net decrease in heat transfer from the wall to the fluid body i.e. lower Nusselt numbers. The opposite trend is achieved for wall mass transfer rate i.e. Sherwood number, with greater wall suction (fig. 12b) wherein it is apparent that greater adherence of the boundary layer to the wall (associated with a deceleration in the flow) while decreasing the species concentration levels in the fluid, induces greater species diffusion flux from the sheet (wall) to the fluid. Under Fick's law of mass diffusion, the mass transfer rate at the wall must therefore increase and this is testified to in fig. 12b. Finally in figs 13a,b, it is apparent that Sherwood number is increased for destructive chemical reaction ($(\gamma)<0$) whereas it is reduced for constructive (generative) reaction ($(\gamma)>0$). Sherwood number is enhanced i.e. mass transfer rate at the wall (sheet) is boosted with greater Schmidt numbers (fig. 13a). Fig 13b indicates that with greater Soret number, there is a noticeable elevation in Sherwood number at all time values. Thermo-diffusion (Soret) therefore promotes species diffusion from the wall (sheet) into the boundary layer. In all the plots shown the FDM solutions are found to corroborate extremely closely with the MAGNETO-FEM and MAG-SPICE NSM solutions.

7. CONCLUSIONS

An implicit finite difference numerical solution has been developed for transient magnetohydrodynamic chemically-reacting radiative fluid flow from an impulsively-started vertical porous sheet. Soret/Dufour, heat generation/absorption, Joule heating and viscous dissipation effects have also been integrated into the mathematical model. Verification of computations has been achieved with two distinct numerical algorithms- variational finite elements (MAGNETO-FEM code) and electrothermal network simulation (MAG-SPICE NSM code). The present solutions have demonstrated that the boundary layer flow is accelerated with increasing thermal radiative flux, Eckert number, heat generation and Soret number whereas the flow is decelerated with greater wall suction, heat absorption, magnetic field and Prandtl number. Temperatures are also observed to be elevated with magnetic parameter, radiation heat transfer, Dufour number, heat generation (source) and Eckert number with the contrary effects computed for increasing suction parameter or Prandtl number. The species concentration is

boosted with Soret number and generative chemical reaction whereas it is depressed with greater wall suction, Schmidt number and destructive chemical reaction parameter. Wall shear stress is found to increase with Eckert number and Soret number but is depressed with greater wall suction. Sherwood number is elevated with suction parameter, Schmidt number, generative chemical reaction parameter and also Soret number. The present investigation is relevant to the simulation of certain electro-conductive polymer processing systems under high temperature. It has demonstrated that the FDM algorithm is very stable and adaptive to nonlinear magnetic materials problems and furthermore that FEM and NSM also provide an excellent platform for advanced simulations in this field. Future studies will extend the present investigation to consider non-Newtonian properties of smart polymers (e.g. poly (ethylene terephthalate)) and will be communicated imminently.

ACKNOWLEDGMENTS

The authors are grateful to both reviewers for their comments which have served to improve the present article.

REFERENCES

- [1] T. Kimura, Study on the effect of magnetic fields on polymeric materials and its application, *Polymer J.*, 35, 823-843 (2003).
- [2] N. Kayukawa, Open-cycle magnetohydrodynamic electrical power generation: a review and future perspectives, *Progress in Energy and Combustion Science*, 30, 33-60 (2004).
- [3] S. E. Ahmed, M.A. Mansour and A. Mahdy, MHD mixed convection in an inclined lid-driven cavity with opposing thermal buoyancy force: Effect of non-uniform heating on both side walls, *Nuclear Engineering and Design*, 265, 938-948 (2013).
- [4] T. Fujino, H. Sugita, M. Mizuno, I. Funaki, M. Ishikawa, Influences of electrical conductivity of wall on magnetohydrodynamic control of aerodynamic heating, *AIAA J. Spacecraft and Rockets*, 43, 63-70 (2006).
- [5] Y. Jaluria, Heat and mass transfer in the extrusion of non-Newtonian materials, *Advances in Heat Transfer*, 28, 145-230 (1996).
- [6] A. Bund, A. Ispas and G. Mutschke, Magnetic field effects on electrochemical metal depositions, *Sci. Technol. Adv. Mater.* 9, 024208 (6pp) (2008).
- [7] R. Aris, *The Mathematical Theory of Diffusion and Reaction in Permeable Catalysts. Volume II: Questions of Uniqueness, Stability and Transient Behaviour*, Clarendon Press, Oxford (1975).
- [8] U. N. Das, R. Dekha, V. M. Soungekar, Effects of mass transfer on flow past an impulsively started infinite vertical plate with constant heat flux and chemical reaction, *Forschung im Ingenieurwesen*, 60, 284-287 (1994).

- [9] M. Ferdows and Q. M. Al-Mdallal, Effects of order of chemical reaction on a boundary layer flow with heat and mass transfer over a linearly stretching sheet, *American J. Fluid Dynamics*, 2, 89-94 (2012).
- [10] O.D. Makinde and O. Anwar Bég, On inherent irreversibility in a reactive hydromagnetic channel flow, *J. Thermal Science*, 19, 72-79 (2009).
- [11] M. J. Uddin, O. Anwar Bég, N. Amran and A.I.M.D. Ismail, Lie group analysis and numerical solutions for magneto-convective slip flow of nanofluid over a moving plate with Newtonian heating boundary condition, *Canadian J. Physics*, 93, 1-9 (2015).
- [12] J. A. Rao, S. Sivaiah, and R. Srinivasa Raju, Chemical reaction effects on an unsteady MHD free convection fluid flow past a semi-infinite vertical plate embedded in a porous medium with heat absorption, *J. Applied Fluid Mechanics*, 5, 63-70 (2012).
- [13] J. Zueco, O. Anwar Bég, T.A. Bég and H.S. Takhar, Numerical study of chemically reactive buoyancy-driven heat and mass transfer across a horizontal cylinder in a high-porosity non-Darcian regime, *J. Porous Media*, 12, 33-51 (2009).
- [14] S. Mukhopadhyay, K. Vajravelu, R. A. Van Gorder, Chemically reactive solute transfer in a moving fluid over a moving surface, *Acta Mechanica*, 224, 513-523 (2013).
- [15] O.D. Makinde, F. Mabood, W.A. Khan and M.S. Tshehl, MHD flow of a variable viscosity nanofluid over a radially stretching convective surface with radiative heat, *J. Molecular Liquids*, 219, 624-630 (2016).
- [16] P. G. Siddheshwar and S. Manjunath, Unsteady convective diffusion with heterogeneous chemical reaction in a plane-Poiseuille flow of a micropolar fluid, *Int. J. Engineering Science*, 38, 765-783 (2000).
- [17] E. Ruckenstein, Effect of unsteady convection on mass transfer accompanied by a chemical reaction, *Chemical Engineering J.*, 2, 164-171 (1971).
- [18] TB Chang, A Mehmood, O. Anwar Bég, M Narahari, MN Islam, F Ameen, Numerical study of transient free convective mass transfer in a Walters-B viscoelastic flow with wall suction, *Comm. Nonlinear Science Numerical Simulation*, 16, 216-225 (2011).
- [19] Puneet Rana, R. Bhargava and O. Anwar Beg, Finite element simulation of unsteady MHD transport phenomena on a stretching sheet in a rotating nanofluid, *Proc. IMECHE- Part N; J. Nanoengineering and Nanosystems*, 227, 77-99 (2013).
- [20] A. Hussanan, Z. ismail, I. Khan and S. Shafie, Unsteady MHD free convection flow in a porous medium with constant mass diffusion and Newtonian heating, *Euro. Physics J. Plus*, 129, 46-55 (2014).
- [21] B. Gebhart, *Heat Conduction and Mass Diffusion*, MacGraw-Hill, New York (1993).
- [22] N. Islam and M. M. Alam, The Dufour and Soret effects on unsteady MHD free convection and mass transfer flow through a porous medium past an infinite vertical porous plate in a rotating system, *Bangladesh J. Scientific Industrial Research*, 43, 159-172 (2008).
- [23] M.A. Mansour, N.F. El-Anssary, A.M. Aly, Effects of chemical reaction and thermal stratification on MHD free convective heat and mass transfer over a vertical stretching surface embedded in a porous media considering Soret and Dufour numbers, *Chemical Engineering J.*, 145, 340-345 (2008).

- [24] V. Ramachandra Prasad, B. Vasu, O. Anwar Bég, Thermo-diffusion and diffusion-thermo effects on MHD free convection flow past a vertical porous plate embedded in a non-Darcian porous medium, *Chemical Engineering J.*, 173, 598–606 (2011).
- [25] O. Anwar Bég, Bakier, A.Y. and V.R. Prasad, Numerical study of free convection magnetohydrodynamic heat and mass transfer from a stretching surface to a saturated porous medium with Soret and Dufour effects, *Computational Materials Science*, 46, 57-65 (2009).
- [26] I.J. Uwanta, K.K. Asogwa, U.A. Ali, MHD fluid flow over a vertical plate with Dufour and Soret effects, *Int. J. Computer Applications*, 45, 8-16 (2012).
- [27] O. Anwar Bég, A. Bakier, V.R. Prasad and S. K. Ghosh, Numerical modelling of non-similar mixed convection heat and species transfer along an inclined solar energy collector surface with cross diffusion effects, *World J. Mechanics*, 1, 185-196 (2011).
- [28] A. Lohmuller, W. Esser, J. Gossmann, M. Hordler, J. Preuhs, and R.F. Singer, *Superalloys 2000*, T.M. Pollock, R.D. Kissinger, R.R. Bowman, K.A. Green, M. McLean, S.L. Olson, and J.J. Schirra, eds., TMS, Warrendale, Pennsylvania, USA, 181–88 (2000).
- [29] McCaffrey, B.J., Quintiere, J.G., Harkelroad, M.F., Estimating room temperatures and the likelihood of flashover, *Fire Technology*, 17, 119 -122 (1981).
- [30] J. Dowden (Ed), *The Theory of Laser Materials Processing: Heat and Mass Transfer in Modern Technology*, Springer, Berlin (2009).
- [31] S. Chandrasekhar, *Radiative Transfer*, Clarendon, Oxford, USA (1961).
- [32] Zhou, Z.Y., Yu, A.B. and Zulli, P, Particle scale study of heat transfer in packed and bubbling fluidized beds, *AIChE J.*, 55, 868-884 (2009).
- [33] O. Anwar Bég, Nasir Ali, Akbar Zaman, Tasveer A. Bég, Computational modelling of heat transfer in annular porous medium solar energy absorber with a Traugott's P1-radiative differential approximation, *AIAA J. Thermophysics Heat Transfer* (2015). Under review
- [34] Traugott, C., Radiative heat-flux potential for a non-gray gas, *AIAA J.*, 4, 541-542 (1966).
- [35] Takhar, H.S., Bég, O. Anwar and Kumari, M., Computational analysis of coupled radiation convection dissipative flow in non-Darcy porous medium using the Keller-Box implicit difference scheme, *Int. J. Energy Research*, 22,141-159 (1998).
- [36] Bég, O. Anwar, J. Zueco, Bég, T. A., H. S. Takhar and E. Kahya NSM analysis of time-dependent nonlinear buoyancy-driven double-diffusive radiative convection flow in non-Darcy geological porous media, *Acta Mechanica*, 202, 181-204 (2009).
- [37] Nagaraju, P., Chamkha, A.J., Takhar, H.S. and Chandrasekhara. B.C.: Simultaneous radiative and convective heat transfer in a variable porosity medium, *Heat and Mass Transfer*, 37, 243-250 (2001).
- [38] Bég, O. Anwar, Bég, T. A., N. Ali and M.N. Islam, Spectral computational simulation of a two-flux radiative model for hypersonic heat transfer from a cone, *ASCE J. Aerospace Engineering* (2015). Submitted
- [39] Bég, O. Anwar and Takhar, H.S., Mathematical Modeling of dissipative Darcy-Forscheimmer flow of convective-radiative viscoelastic flow in non-Darcy porous medium using

the Rossleand radiative transfer model, *5th World Congress on Computational Mechanics, Vienna University of Technology, Wein, Vienna, Austria, July (2002).*

[40] Bég, O. Anwar, J. Zueco, H.S. Takhar, T.A. Bég, A. Sajid, Transient nonlinear optically-thick radiative–convective double-diffusive boundary layers in a Darcian porous medium adjacent to an impulsively started surface–Network simulation solutions, *Comm. Nonlinear Science and Numerical Simulation*, 14, 3856-3866 (2009).

[41] M.F. Modest, *Radiation Heat Transfer*, MacGraw-Hill, New York (1993).

[42] R. D. Cess, The interaction of thermal radiation with free convection heat transfer, *Int. J. Heat Mass Transfer*, 9, 1269–1277 (1966).

[43] K.H. Lee and R. Viskanta, Comparison of the diffusion approximation and the discrete ordinates method for the investigation of heat transfer in glass, *Glass Science and Tech.*, 72, 254-265 (1999).

[44] M. A. Hossain, H. S. Takhar, Radiation effects on mixed convection along a vertical plate with uniform surface temperature, *Heat Mass Transfer*, 31, 243–248 (1996).

[45] Md. Jashim Uddin, O. Anwar Bég and Ahmad Izani Md. Ismail, Mathematical modelling of radiative hydromagnetic thermo-solutal nanofluid convection slip flow in saturated porous media, *Math. Prob. Eng.*, Article ID 179172, 11 pp doi.org/10.1155/2014/179172 (2014)

[46] M Ferdows, MS Khan, O. Anwar Bég, MAK Azad, MM Alam, Numerical study of transient magnetohydrodynamic radiative free convection nanofluid flow from a stretching permeable surface, *Proc. IMechE-Part E: J. Process Mechanical Engineering*, 228 (3) 181-196 (2014).

[47] T. Hayat, M. Mustafa, M. Sajid, Influence of thermal radiation on Blasius flow of a second grade fluid, *Z. Naturforsch.*, 64a, 827-833 (2009).

[48] O. Anwar Bég, M. J. Uddin, M.M. Rashidi, and N. Kavyani, Double-diffusive radiative magnetic mixed convective slip flow with Biot and Richardson number effects, *J. Engineering Thermophysics*, 23 (2), 79-97 (2014).

[49] Sattar, M. A., Kalim, H., Unsteady free-convection interaction with thermal radiation in a boundary layer flow past a vertical porous plate, *J. Math. Phys. Sci.*, 30, 25- 37 (1996).

[50] O. Atdin and A. Kaya, Radiation effect on MHD mixed convection flow about a permeable vertical plate, *Heat and Mass Transfer*, 45, 239-246 (2008).

[51] S. Shateyi, S.S. Motsa and P. Sibanda, The effects of thermal radiation, Hall currents, Soret, and Dufour on MHD flow by mixed convection over a vertical surface in porous media, *Mathematical Problems in Engineering*, vol. 2010, Article ID 627475, 20 pages (2010). [doi:10.1155/2010/627475](https://doi.org/10.1155/2010/627475).

[52] Olanrewaju, P.O., Gbadeyan, J.A., Effects of Soret, Dufour, chemical reaction, thermal radiation and volumetric heat generation/absorption on mixed convection stagnation point flow on an isothermal vertical plate in porous media, *Pacific J. Science Technology*, 11, 1-12 (2010).

[53] Carnahan B, Luther HA, Wilkes JO., *Applied Numerical Methods*, John Wiley and Sons, New York (1969).

[54] J.N. Reddy, *The Finite Element Method*, MacGraw-Hill, USA (1985).

- [55] O. Anwar Bég, J. Zueco and L. M. López-Ochoa, Network numerical analysis of optically-thick hydromagnetic slip flow from a porous spinning disk with radiation flux, variable thermophysical properties and surface injection effects, *Chemical Engineering Communications*, 198, 360-384 (2011).
- [56] F. Mabood, W.A. Khan and A.I.Md. Ismail, MHD stagnation point flow and heat transfer impinging on stretching sheet with chemical reaction and transpiration, *Chemical Engineering J*, 273, 430-437 (2015).
- [57] F. Mabood, W.A. Khan and A..I.Md. Ismail, MHD boundary layer flow and heat transfer of nanofluids over a nonlinear stretching sheet: A numerical study, *J. Magnetism and Magnetic Materials*, 374, 569-576. (2015).
- [58] F. Mabood, W.A. Khan and A.I.Md. Ismail, Multiple slips effects on MHD Casson fluid flow in porous media with radiation and chemical reaction, *Canadian J. Physics*, 94, 26-34 (2016).
- [59] F. Mabood, W.A. Khan Homotopy analysis method for boundary layer flow and heat transfer over a permeable flat plate in a Darcian porous medium with radiation effects, *J. Taiwan Institute of Chemical Engineers*, 45, 1217-1224 (2014).
- [60] H.S. Takhar and O. Anwar Bég, Effects of transverse magnetic field, Prandtl number and Reynolds number on non-Darcy mixed convective flow of an incompressible viscous fluid past a porous vertical flat plate in saturated porous media, *Int. J. Energy Research*, 21, 87-100 (1997).
- [61] M.Q. Brewster, *Thermal Radiative Transfer and Properties*, John Wiley and Sons Inc., New York, USA (1992).
- [62] S.S. Rao, *The Finite Element Method in Engineering*, MacGraw-Hill, New York (1985).
- [63] D. Gupta, Lokendra Kumar, O. Anwar Bég and Bani Singh, Finite element simulation of mixed convection flow of micropolar fluid over a shrinking sheet with thermal radiation, *Proc IMechE- Part E: J. Process Mechanical Engineering*, 228 (1) 61-72 (2014). DOI: 10.1177/0954408912474586.
- [64] O. Anwar Bég, Tasveer A. Bég, R. Bhargava, S. Rawat and D. Tripathi, Finite element study of pulsatile magneto-hemodynamic non-Newtonian flow and drug diffusion in a porous medium channel, *J. Mechanics in Medicine and Biology*, 12 (4) 1250081.1 – 1250081.26 (2012).
- [65] Diksha Gupta, Lokendra Kumar, O. Anwar Bég and Bani Singh, Finite element simulation of nonlinear magneto-micropolar stagnation point flow from a porous stretching sheet with prescribed skin friction, *Computational Thermal Sciences*, 7 (1): 1–14 (2015).
- [66] V. Rajesh, O. Anwar Bég and M. P. Mallesh, Transient nanofluid flow and heat transfer from a moving vertical cylinder in the presence of thermal radiation: Numerical study, *Proc. IMechE-Part N: J. Nanoengineering Nanosystems*, 14 pp. DOI: 10.1177/1740349914548712 (2014).
- [67] P. Rana, R. Bhargava and O. Anwar Bég, Finite element modeling of conjugate mixed convection flow of Al₂O₃-water nanofluid from an inclined slender hollow cylinder, *Physica Scripta*, 88 (2013) (15pp).
-

- [68] L. W. Nagel, SPICE2: A computer program to simulate semiconductor circuits, *Electronics Research Laboratory Report #ERL-M520, University of California, Berkeley, USA, May (1975)*.
- [69] J. Zueco and O. Anwar Bég, Network numerical analysis of hydromagnetic squeeze film flow dynamics between two parallel rotating disks with induced magnetic field effects, *Tribology International*, 43, 532-543 (2010).
- [70] O. Anwar Bég, J. Zueco, M. Norouzi, M. Davoodi, A. A. Joneidi, Assma F. Elsayed, Network and Nakamura tridiagonal computational simulation of electrically-conducting biopolymer micro-morphic transport phenomena, *Comp. Biol.Medicine*, 44, 44–56 (2014).
- [71] O. Anwar Bég and T. A. Bég, Network and finite element simulation of electro-rheological smart dampers for seismic applications, *Technical Report GEO-ELECTRO-4/13, 65pp Gort Engineering, Bradford and Manchester, UK, July (2013)*.
- [72] O. Anwar Bég and T. A. Bég, Network electrothermal model for electro-kinetic stabilization of geotechnical embankments under severe weather, *Technical Report GEO-ELECTRO-2/13, 58pp Gort Engineering, Bradford and Manchester, UK, March (2013)*.
- [73] Z. Dursunkaya, W.M. Worek, Diffusion-thermo and thermal diffusion effects in transient and steady natural convection from a vertical surface, *Int. J. Heat Mass Transfer*, 35, 2060–2065, (1992).
- [74] W.E. Stewart Jr., A.S. Burns, Convection in a concentric annulus with heat generating porous media and a permeable inner boundary, *Int. Comm. Heat Mass Transfer*, 19, 859-868 (1992).
- [75] H. Schlichting, *Boundary-Layer Theory*, MacGraw-Hill, New York, 8th edn (2000) .
- [76] B. Gebhart, Effects of viscous dissipation in natural convection, *J. Fluid Mech.*, 14, 225-232 (1962).
- [77] B. Gebhart and J. Mollendorf, Viscous dissipation in external natural convection flows. *J. Fluid Mech*, 38, 97-107 (1969).
- [78] J. A. Weaver and R. Viskanta, Natural convection due to horizontal temperature and concentration gradients (2): species inter-diffusion, Soret and Dufour effects, *Int. J. Heat Mass Transfer*, 34, 3121–3133 (1991).
- [79] M.A. Chaudhary and J.H. Merkin, A simple isothermal model for homogeneous–heterogeneous reactions in boundary-layer flow I. Equal diffusivities, *Fluid Dyn Res*, 16, 311-333 (1995).
-

FIGURES

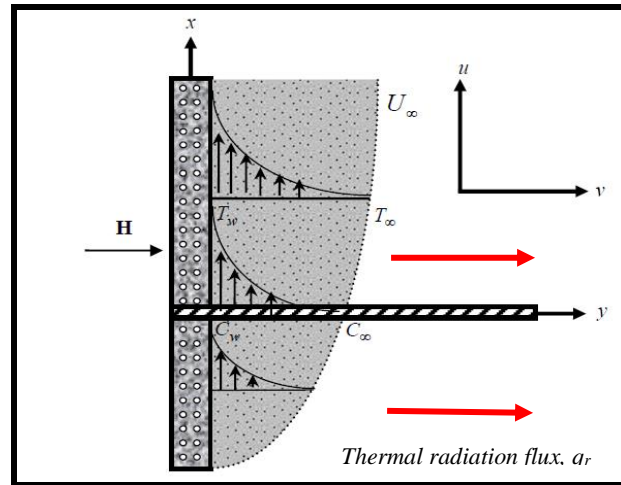


Fig. 1 Physical model for thermal radiative magnetic materials sheet processing system

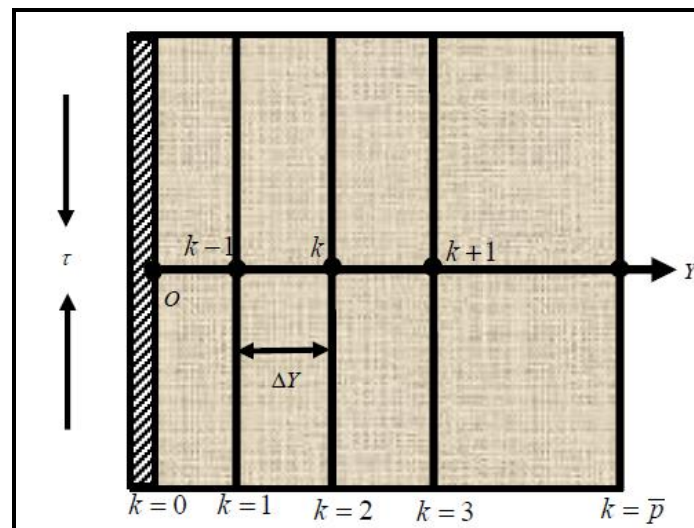


Fig. 2. Implicit finite difference system grid (mesh)

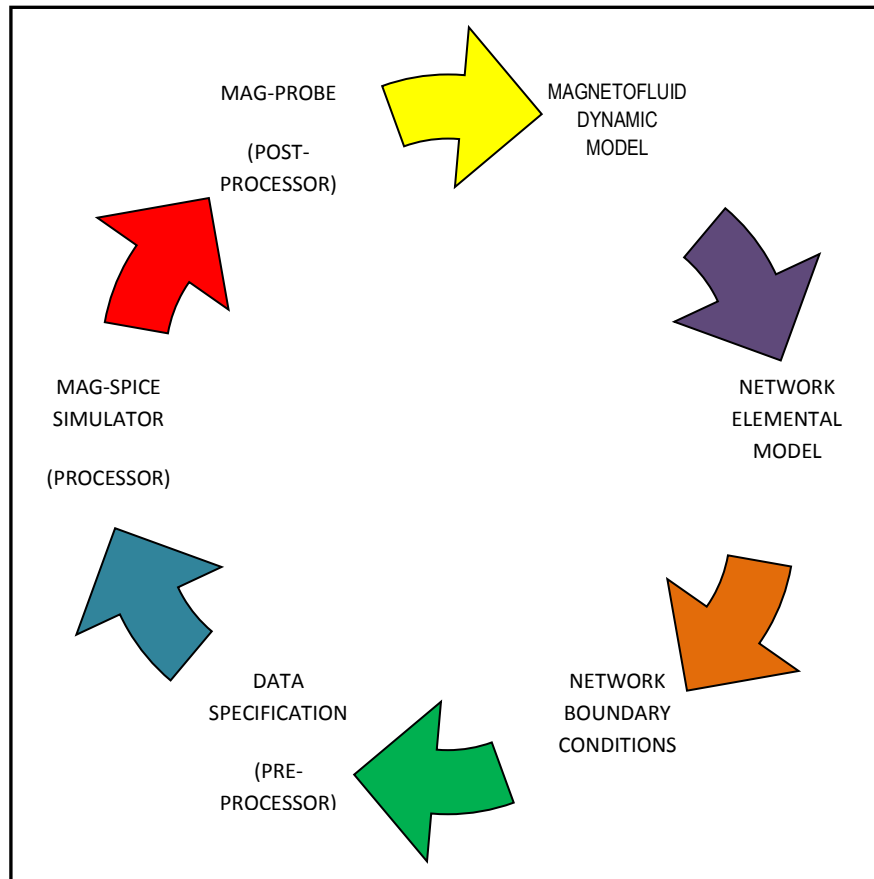


Fig. 3: MAG-PSPICE network simulation methodology

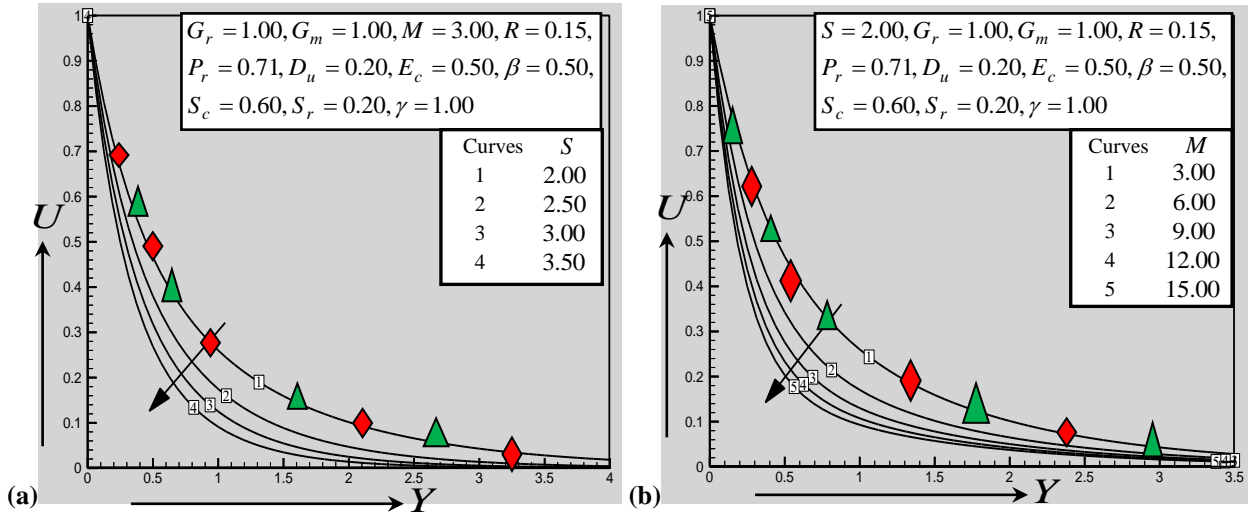


Fig. 4. FDM solutions for velocity for various values of (a) Suction parameter, S and (b) Magnetic parameter, M respectively (N.B. green triangle = MAGNETO-FEM solution, red diamond = MAG-SPICE NSM solution here and in all other figures for appropriate FDM case validation).

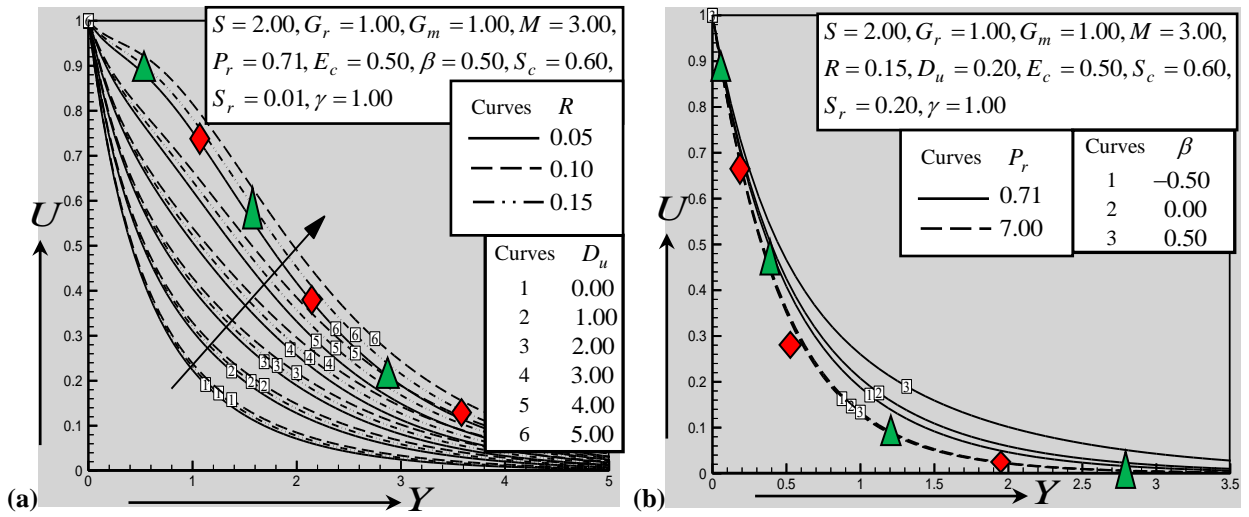


Fig. 5. FDM solutions for velocity for various values of (a) Radiation-conduction parameter, R and Dufour number, D_u and (b) Prandtl number, P_r and Heat generation/absorption parameter, β respectively.

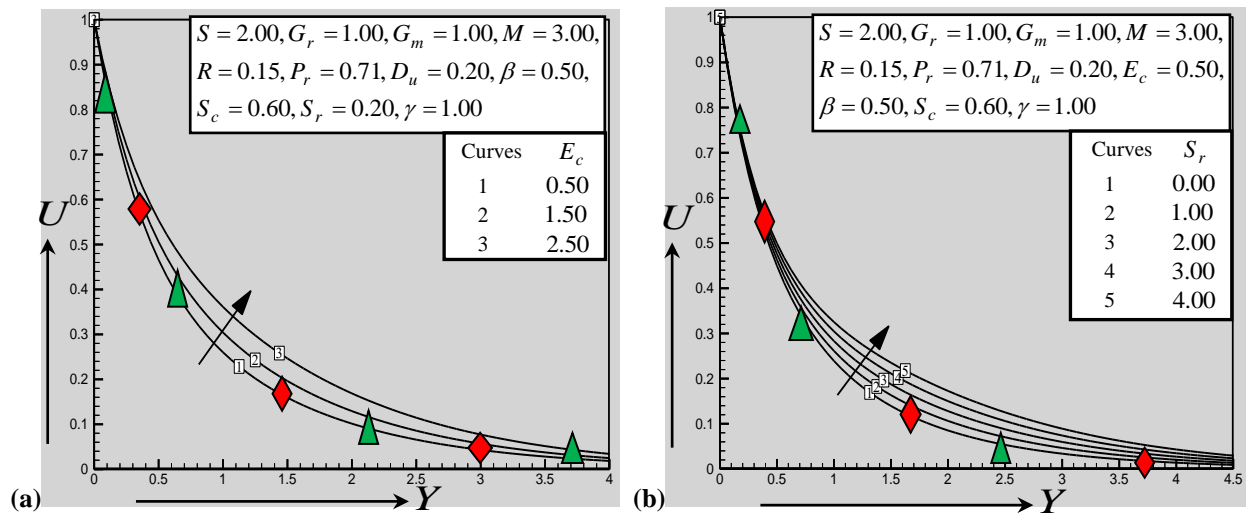


Fig. 6. FDM solutions for velocity with various values of (a) Eckert number, E_c and (b) Soret number, S_r respectively.

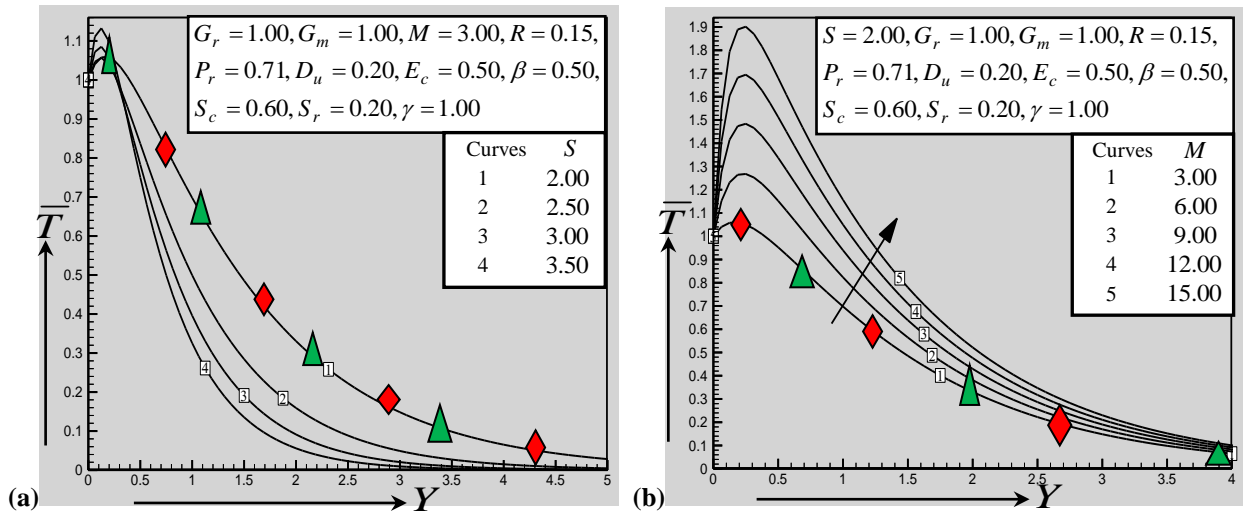


Fig. 7. FDM solutions for temperature evolution with various values of (a) Suction (lateral wall mass flux) parameter, S and (b) Magnetic parameter, M respectively.

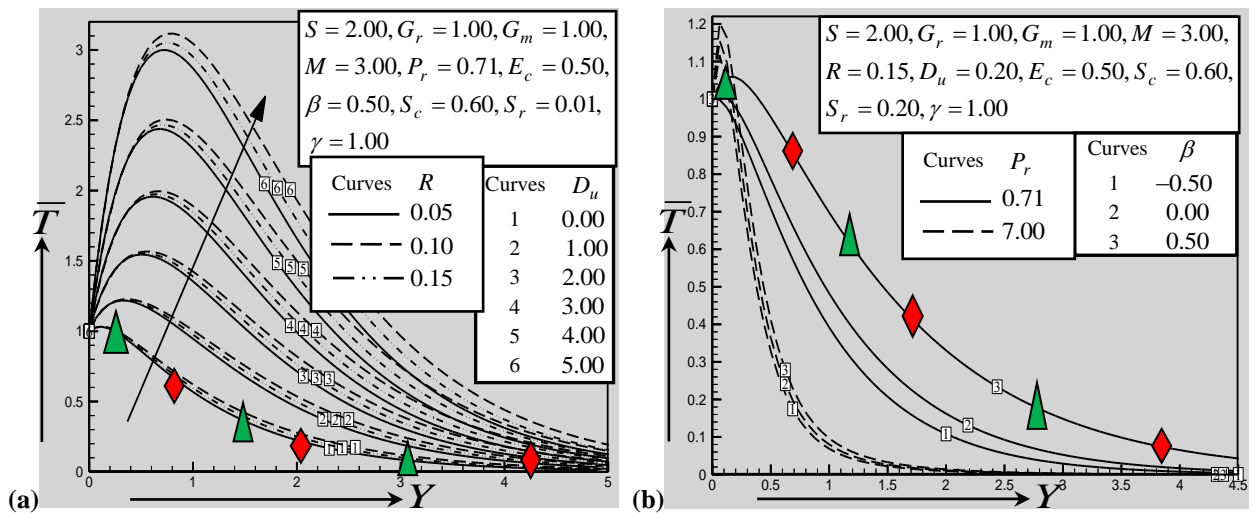


Fig. 8. FDM solutions for temperature evolution with various values of (a) Radiation-conduction parameter, R and Dufour number, D_u and (b) Prandtl number, P_r and Heat generation/absorption parameter, β respectively.

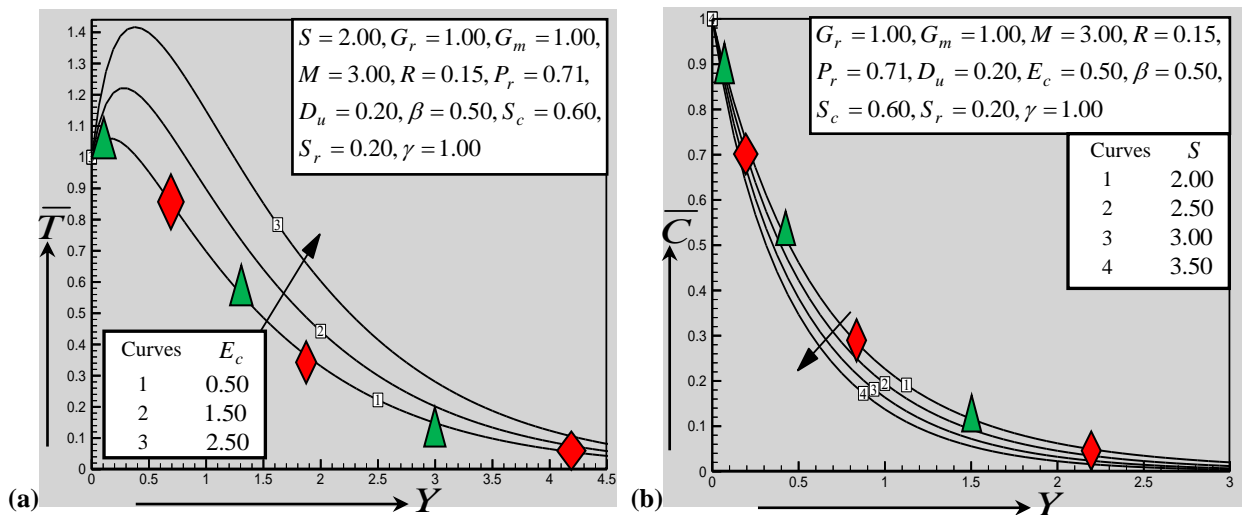


Fig. 9. FDM solutions for (a) temperature evolution with various values of Eckert number, E_c and (b) concentration distribution with various values of Suction (lateral wall mass flux) parameter, S respectively.

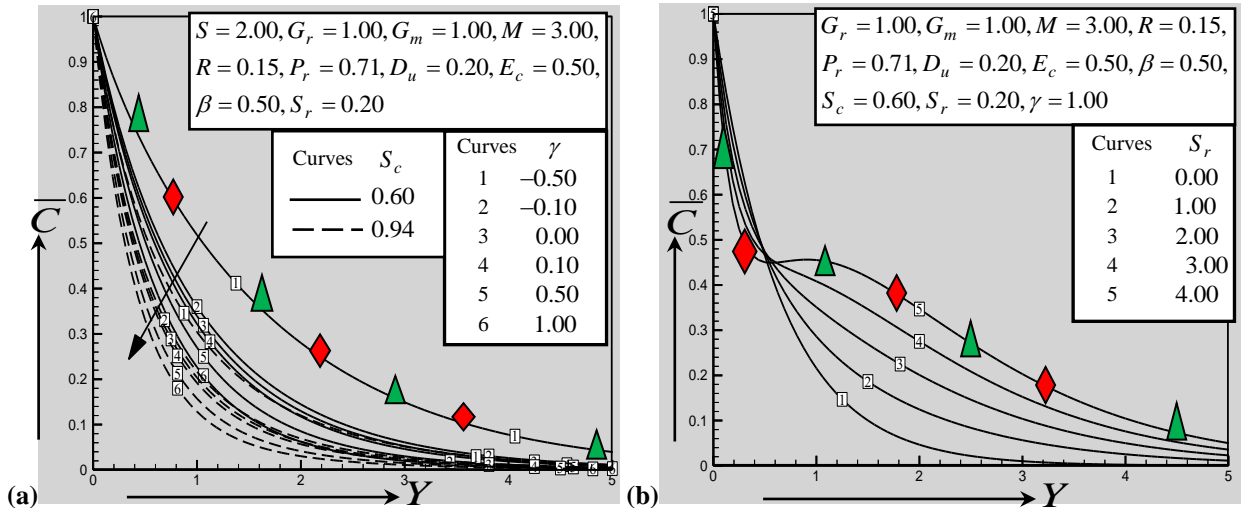


Fig. 10. FDM solutions for concentration distribution with various values of (a) Schmidt number, S_c and Chemical reaction parameter and (b) Soret number S_r respectively.

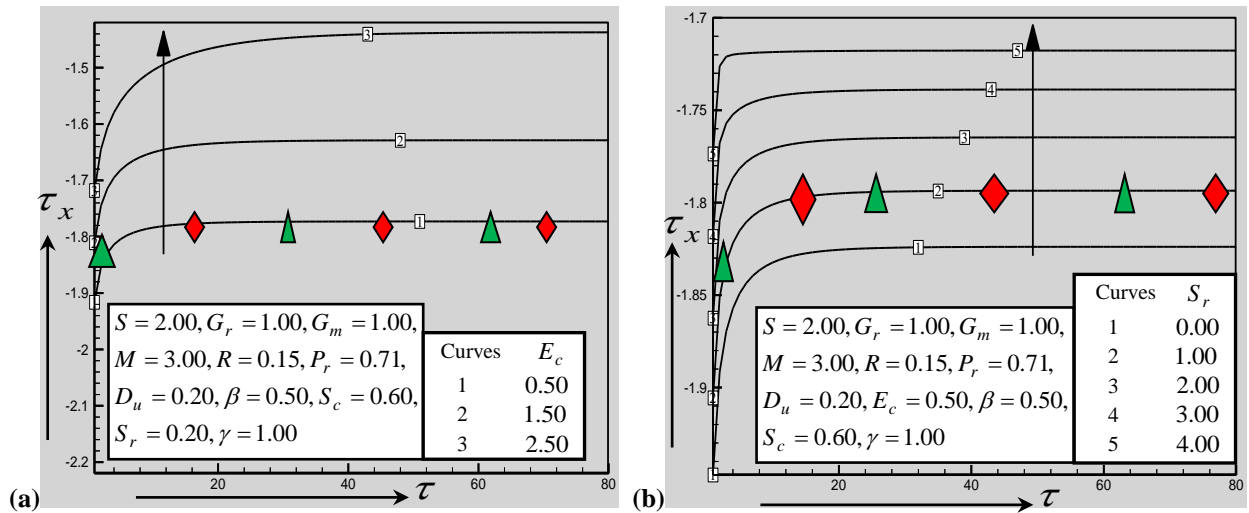


Fig. 11. Transient FDM solutions for shear stress distribution with various values of (a) Eckert number, E_c and (b) Soret number, S_r respectively.

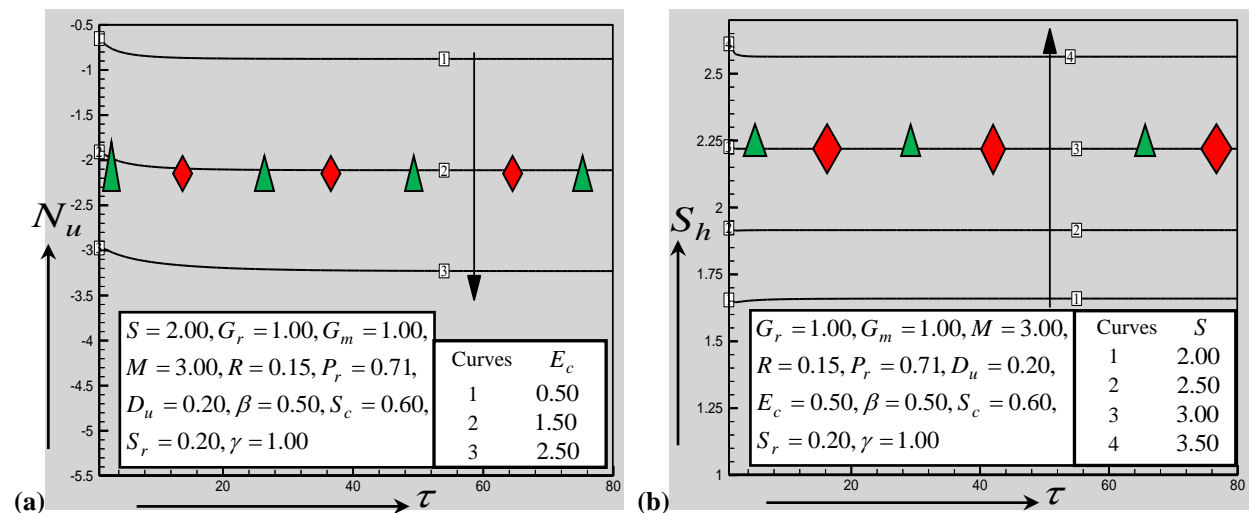


Fig. 12. Transient FDM solutions for (a) Nusselt number with various values of Eckert number, E_c and (b) Sherwood number for various values of Suction (lateral wall mass flux) parameter, S respectively.

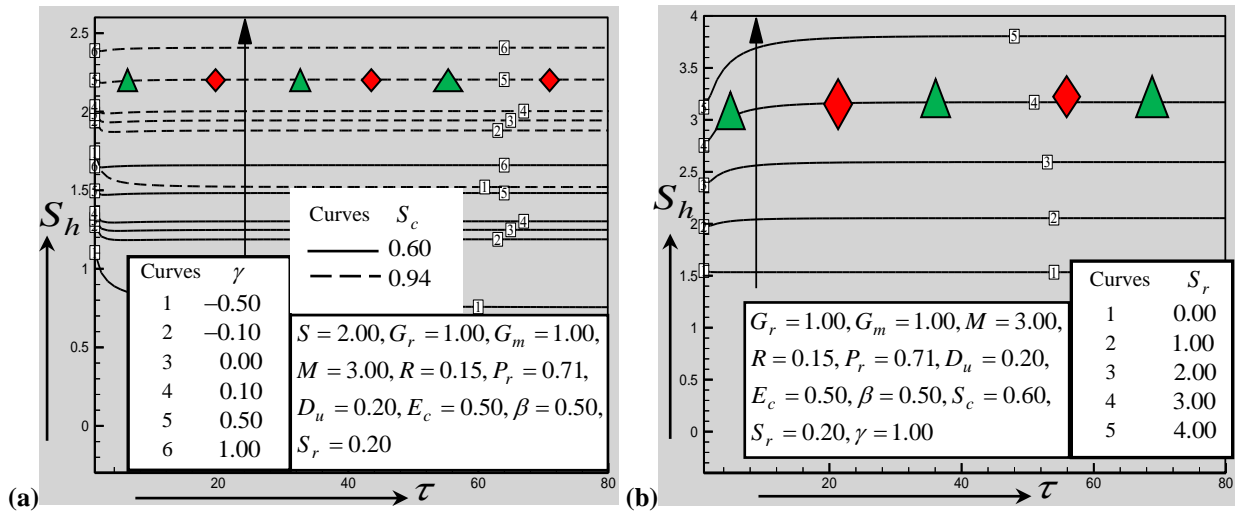


Fig. 13. Transient FDM solutions for Sherwood number with various values of (a) Schmidt number, S_c and Chemical reaction parameter and (b) Soret number S_r , respectively.

TABLES

FDM	MAGNETO-FEM	MAG-SPICE	GRID SIZE (Y direction)
0.2388	0.2378	0.2391	50
0.2444	0.2452	0.2456	75
0.2601	0.2602	0.2604	100
0.2601	0.2602	0.2604	120

Table 1: Grid refinement for steady state U (velocity) solution with different numerical schemes at $\tau=15$ and $Y = 1$ with $G_r=1, G_m=1, M = 3, R = 0.15, P_r=0.71, D_u = 0.2, E_c = 0.5, \beta = 0.5, S_c=0.6, S_r = 0.2, S = 2.0$ and $\gamma=1.0$.